A novel non-genetic murine model of hyperglycemia and hyperlipidemia-associated accelerated atherosclerosis

Susanne Gaul[1]*, PhD; Khurrum Shahzad[2]*, PhD; Rebekka Medert[3,5]*, PhD; Ihsan Gadi[2], Christina Mäder[1], Dagmar Schumacher, PhD[3, 5]; Angela Wirth[3], PhD; Saira Ambreen[2], Sameen Fatima[2], Jes-Niels Boeckel[1], PhD, Hamzah Khawaja[2], Jan Haas[4,5], PhD; Maik Brune[6], MD; Peter P Nawroth[6], Prof., MD; Berend Isermann[2#], Prof., MD; Ulrich Laufs[1#], Prof., MD; Marc Freichel[3, 5#], Prof., MD

[1] Klinik und Poliklinik für Kardiologie, Universitätsklinikum Leipzig, Leipzig, Germany

[2] Laboratory Medicine, Clinical Chemistry and Molecular Diagnostic, University Hospital Leipzig, Leipzig, Germany

[3] Institute of Pharmacology, Heidelberg University, Heidelberg, Germany

[4] Department of Internal Medicine III, Heidelberg University, Heidelberg, Germany

[5] DZHK (German Centre for Cardiovascular Research), partner site Heidelberg/Mannheim, Germany

[6] Internal Medicine I and Clinical Chemistry, German Diabetes Center (DZD), Heidelberg University, Heidelberg, Germany

*equally contributing first author; [#] equally contributing last author

Corresponding authors:

Khurrum Shahzad

Institute of Laboratory Medicine, Clinical Chemistry and Molecular Diagnostic, University Hospital, Leipzig, Liebigstr.27, Leipzig 04103, Germany,

Email: khurrum.shahzad@medizin.uni-leipzig.de

Marc Freichel

Institute of Pharmacology, Heidelberg University, Im Neuenheimer Feld 366, 69120 Heidelberg, Germany;

Email: marc.freichel@pharma.uni-heidelberg.de

Abstract

Objective: Atherosclerosis, the main pathology underlying cardiovascular diseases is accelerated in diabetic patients. Genetic mouse models require breeding efforts which are time-consuming and costly. To establish a new non-genetic model of inducible metabolic risk factors mimicking hyperlipidemia, hyperglycemia, or both and allowing to detect phenotypic differences dependent on the metabolic stressor(s).

Methods and Results: Wild type mice were injected with gain-of-function PCSK9^{D377Y} (proprotein convertase subtilisin/kexin type 9) mutant adeno-associated viral particles (AAV) and streptozotocin and fed either a high-fat diet (HFD) or high-cholesterol/high fat-diet (Paigen diet, PD). Combined hyperlipidemic and hyperglycemic (HGHCi) mice, but not hyperlipidemia (HCi) alone, display characteristic features of accelerated atherosclerosis. Atherosclerotic plaques of HGHCi animals were larger, showed a less stable phenotype, contained more macrophages and less smooth muscle cells. These findings were observed both at early (12 weeks) and late (20 weeks) time points on both HFD or PD diet. Differences between the HGHCi and HCi model were confirmed using RNAseq analysis revealing that significantly more genes are dysregulated in mice with combined hyperlipidemia and hyperglycemia as compared to the hyperlipidemia only group. The HGHCi-associated genes were related to pathways regulating inflammation, cellular metabolism and collagen degradation. PD accelerates atherosclerosis in mice and shows plaque formation already after 8 weeks, therefore, representing a fast direct inducible hyperglycemic atherosclerosis model.

Conclusion: We established a non-genetic inducible mouse model allowing comparative analyses of atherosclerosis in HCi and HGHCi conditions and its modification by diet, allowing analyses of multiple metabolic hits in mice.

Keywords: animal model of disease, atherosclerosis, diabetes, hyperglycemia, hyperlipidemia, PCSK9, Streptozotocin

Nonstandard Abbreviations and Acronyms

ApoE	apolipoprotein E
BSA	bovine serum albumin
BCA	bicinchoninic acid
DM	diabetes mellitus
DAPI	4',6-Diamidino-2-Phenylindole, Dihydrochloride
HFD	high fat diet
HRP	horseradish peroxidase
LDLR	low-density lipoprotein receptor
NOD	non-obese diabetic
OCT	optimal cutting temperature
PD	paigen diet
PCSK9	proprotein convertase subtilisin/kexin type 9
PBS	phosphate buffer saline
RIPA	radioimmunoprecipitation assay
RNAseq	RNA sequencing
rAAV	recombinant adeno-associated virus
STZ	streptozotocin
α-SMA	α smooth muscle actin

Introduction

Atherosclerotic cardiovascular diseases including coronary artery disease (CAD) and its complications are a leading cause of mortality and morbidity globally [1]. The risk of CAD is markedly increased in patients with both type 1 and type 2 diabetes mellitus (DM), with CAD events occurring earlier in patients with diabetes mellitus[2]. About 10 % of total vascular deaths have been attributed to diabetes mellitus and its complications[2]. Despite recent studies showing cardioprotective effects of new antidiabetic agents[3], there is high need to understand how diabetes associated alterations, particularly chronic hyperglycemia and metabolic alterations evoked thereby, aggravates atherosclerosis in CAD patients as basis for the development of more effective treatments for these high risk patients.

Currently used mouse models of hyperglycemia-associated atherosclerosis require a combination of streptozotocin (STZ) and crossbreeding with either Apolipoprotein E ($ApoE^{-/-}$) or low density lipoprotein receptor ($LDLR^{-/-}$) genetic knock-out mice, or alternatively, a double crossbreeding of $ApoE^{-/-}$ or $LDLR^{-/-}$ with insulin receptor ($Ins2^{+}$, Akita) mutant mice[4]. Some murine models such as STZ-injected human apoB-expressing transgenic mice[5] or the non-obese diabetic (NOD) mice[6] are resistant to the development of atherosclerosis. In addition, crossing of mouse lines is time-consuming and costly. In particular, if mouse models harbouring other genetic manipulations are to be used, backcrossing becomes a major issue. Thus, there is a high demand to generate an inducible mouse model of multiple metabolic hits, e.g. hyperlipidemia and hyperglycemia, which can be used alone or in combination with other genetic modifications. Bjorklund et al. developed a non-genetic mouse model of atherosclerosis induced by a single injection of recombinant adeno-associated virus (rAAV) encoding a hyperactive proprotein convertase subtilisin/kexin type 9 $(PCSK9)^{D377Y}$ mutant followed by high-fat diet feeding that has been used in non-diabetic settings[7, 8] as well as in mature diabetic Akita mice where they showed diabetic- associated accelerated atherosclerosis[7]. Here, we combined injections of rAAV8-$PCSK9^{D377Y}$ and STZ followed by high-fat diet (HFD) feeding to generate a rapid and versatile method to induce a hyperglycemia- accelerated mouse model of atherosclerosis.

Materials and Methods

All informations regarding material and reagents are listed in the major resources table.

Reagents

The following antibodies were used in the current study: rabbit anti-LDLR (R&D Systems, United States), mouse anti-β actin (Abcepta Inc. United States), goat anti-rabbit IgG HRP (Cell Signaling Technology, Germany), rat anti-MOMA-2, rabbit anti-CD68 and rabbit anti- alpha smooth muscle actin (α-SMA) (abcam, Germany), rabbit anti-GAPDH (Sigma-Aldrich,

118 Germany). The following secondary antibodies for immunofluorescence were used: Texas red
119 rabbit anti-mouse IgG (Vector Laboratories, United States), Goat anti-Rat IgG (H+L) Cross-
120 Adsorbed Secondary Antibody, Alexa Fluor 568 (ThermoFisher, United States). Other
121 reagents were as follows: BCA reagent (Perbio Science, Germany); vectashield mounting
122 medium with DAPI (Vector Laboratories, United States); nitrocellulose membrane (Bio-Rad,
123 USA) and immobilon™ western chemiluminescent HRP substrate (Merck, Millipore, United
124 States); streptozotocin (Enzo Life Sciences, Germany); Oil-Red O (Sigma-Aldrich, Germany);
125 accu-chek test strips, accu-check glucometer, protease inhibitor cocktail (Roche Diagnostics,
126 Germany); albumin fraction V, hematoxylin Gill II, acrylamide, agarose (Carl ROTH, Germany);
127 aqueous mounting medium (ZYTOMED, Germany); "high fat diet" (HFD) experimental food
128 (Western-type diet containing 21 % fat and 0.21 % cholesterol or paigen diet containing 16 %
129 fat, 1.25 % cholesterol, and 0.5 % sodium cholate, Ssniff, Germany); PBS (Life Technologies,
130 Germany); rompun 2 % (Bayer, Germany); ketamine 10 % (beta-pharm, Germany).
131
132 **Mice**
133 Eight weeks old male LDLR$^{-/-}$ (002207) mice were obtained from the Jackson Laboratory (Bar
134 Harbor, ME, USA). Male wild-type C57BL/6N were obtained from Charles River Laboratories
135 (Wilmington, MA, USA). Only age-matched male mice were used throughout the study (6-7
136 mice per group). All animal experiments comply with the ARRIVE guidelines and are carried
137 out in accordance with the Directive 2010/63/EU guidelines. They were conducted following
138 standards and procedures approved by the local Animal Care and Use Committee (35-
139 9185.81/G-185/19, Regierungspräsidium Karlsruhe, Germany).
140
141 **Generation and quantification of rAAV8 viral particles**
142 Recombinant rAAV8 vector particles were generated and purified using the iodixanol gradient
143 ultracentrifugation method[9, 10]. The rAAV8 production was carried out using HEK293T cells.
144 First, 1.8x10^{8} HEK293T cells were seeded in a ten chamber CellStack (Corning, USA) and
145 cultured in DMEM+ Glutamax (Gibco, Thermo Fisher Scientific, USA) supplemented with 10%
146 fetal bovine serum (FBS) and 1% penicillin G / streptomycin. After 48 hours, a 1:1:1 molar ratio
147 of pAAV-D377YmPCSK9-bGHpA plasmid[7], the rep-cap AAV8 helper plasmid and an
148 adenoviral helper plasmid was mixed and transfected using polyethylenimine (PEI)
149 (Polyscience, USA). The cells were harvested in 3 ml lysis buffer and lysed by four freeze-
150 thaw cycles 72 hours after transfection. The vector particles were purified using an iodixanol
151 (Progen, Germany) gradient consisting of four phases with decreasing density (60%, 40%,
152 25%, 15%) and ultracentrifugation at 50,000 x g for 135 min at 4°C. Approximately 3 ml of the
153 40% phase, in which predominantly full virus particles accumulate, were recovered with a 27G
154 needle. Finally, the vector solution was buffered into PBS using dialysis tubes (Zeba Spin

155 Desalting Columns 7K MWCO, Thermo Scientific, USA) and concentrated (VivaSpin 10K
156 MWCO, Sartorius, Germany). Vector titer was quantified as genome copy numbers per ml
157 using a qPCR SYBR-Green assay (Biorad) and primers sequences which are specific for the
158 bGHpA sequence (bGHpA-fw 5´ACCTAACTCACTGATCCGAAATTA 3´, bGHpA-rev
159 5´ATTTCGGATCAGTGAGTTAGG 3´)[11].
160
161 **Induction of atherosclerosis by hypercholesterolemia (HCi) and hypercholesterolemia**
162 **and hyperglycemia (HGHCi) in mice**
163 Adeno-associated viral vectors encoding the gain-of-function variant D377Y of the murine
164 PCSK9 (rAAV8-PCSK9^{D377Y}) under the control of liver-specific promoter were delivered via a
165 single retro-orbital sinus injection (1.0 x10^{11} viral genomes/mouse), and treated animals were
166 either fed high-fat Western-type diet (HFD, containing 21 % fat and 0.21 % cholesterol), a high-
167 cholesterol/high-fat Paigen diet (PD, containing 16 % fat, 1.25 % cholesterol, and 0.5 %
168 sodium cholate) to induce chronic hypercholesterolemia (HCi). Control animals not treated with
169 rAAV8-PCSK9^{D377Y} were fed a high-fat diet (graphic abstract).
170 To induce chronic hyperglycemia and hypercholesterolemia (HGHCi), mice were injected with
171 streptozotocin (STZ, 60 mg/kg, intraperitoneally, once daily for five consecutive days, freshly
172 dissolved in 0.05 M sterile sodium citrate, pH 4.5) one week after rAAV8-PCSK9^{D377Y}
173 application. As control for STZ injections mice received injections with equal volume of 0.05 M
174 sodium citrate, pH 4.5 for 5 days. As PCSK9 expression leads to degradation of low density
175 lipoprotein (LDL) receptors, we quantitatively compared the development of atherosclerotic
176 plaque formation in the inducible HCi and HGHCi models with LDLR$^{-/-}$ mice fed HFD or PD.
177 LDLR$^{-/-}$ mice served as the established control model for hypercholesterolemia evoked
178 atherosclerosis[12]. Blood glucose levels were monitored twice a week using Accu-Chek Aviva
179 system (Roche, USA) and maintained in a range of 300–500 mg/dl. Body weight was
180 measured once weekly. HFD and/or hyperglycemia (minimum 300 mg/dl) was maintained for
181 up to 12 or 20 weeks. In the first 4 weeks of the study some mice in the PD as well as in the
182 HFD groups did not tolerate the food. These animals showed a strong reduction in body weight,
183 which is defined as a termination criterion. Consequently, these mice were removed from the
184 study. Mice fed the PD were analysed already after 8-9 weeks due to early mortality in the
185 hyperglycemic group (**Supplementary Figure I**). At respective study endpoints, mice were
186 sacrificed and atherosclerotic plaque morphology was analysed as previously described[13–
187 15].
188 Total plaque size (%) is defined as the size of the plaque comprising all parts of the
189 atherosclerosis (fibrous cap, necrotic tissue, fibrous tissue etc.) within the vessel lumen.
190 Necrotic core (in %) is defined as the area stained blue upon MOVATs pentachrome staining
191 and is presented as the percentage of the total plaque size. Fibrous cap thickness (in µm) is

192 the minimal thickness of the fibrous tissue overlaying a necrotic core. If multiple necrotic cores
193 are present within one plaque, the thickness of all fibrous caps is determined and the average
194 was used for further analyses. Thickness was measured using ImageJ sofware using free-
195 hand tool [13, 14].
196
197 **Analysis of mice**
198 At the end of study period (12 or 20 weeks for HFD or 8 weeks for PD) body weight was
199 measured and mice were sacrificed[14–16]. Blood samples were obtained from the inferior
200 vena cava of anticoagulated mice (500 U unfractionated heparin, intraperitoneally). Blood was
201 centrifuged at 2,000 x g for 20 min at 4°C and plasma was snap frozen in liquid nitrogen. Mice
202 were perfused with ice-cold PBS for 10 min and the heart, aortic arches, including
203 brachiocephalic arteries, were embedded in O.C.T. compound and snap frozen.
204 Brachiocephalic arteries (from distal to proximal) and upper hearts (aortic roots) were
205 sectioned at 5 and 10 µm thickness, respectively.
206
207 **Analysis of plasma lipids**
208 Heparin plasma was prepared for the measurement of plasma lipids. A total of 500 – 700 µl
209 blood per mouse was collected in heparin tubes and centrifuged at 3,500 x g for 10 min at
210 room temperature. Plasma was transferred in a 1.5 ml tube and stored at -80°C. Plasma
211 samples of HFD and PD fed mice were diluted 1:5 with 0.9% NaCl before cholesterol and
212 triglycerides measurements. Plasma samples were analyzed in the accredited central
213 laboratory of the Heidelberg University hospital using standard operating procedures according
214 to the manufacturers' instructions. Cholesterol and triglycerides were analyzed on a Siemens
215 ADVIA Chemistry XPT System (reagents kits 04993681 and 10697575, respectively).
216
217 **Histology**
218 Oil- Red O staining was conducted on frozen sections of the aortic roots or brachiocephalic
219 arteries[14, 17]. Cryopreserved sections of the brachiocephalic arteries and aortic roots (5 and
220 10 µm respectively) were fixed in ice cold acetone for 2 min, rinsed twice in ice cold 1 x PBS,
221 and were stained with Oil- Red O for 10 min. Sections were rinsed twice with distilled water for
222 20 seconds and once in running tap water for 10 min. Sections were then counterstained with
223 haematoxylin for 40 seconds, rinsed in tap water, and mounted with aqueous mounting
224 medium. MOVAT's stain was performed on frozen sections of brachiocephalic arteries. Frozen
225 sections (5 µm) were fixed in Bouin's solution at 50°C for 10 min and stained with 5 % sodium
226 thiosulfate for 5 min, 1 % alcian blue for 15 min, alkaline alcohol for 10 min, Movat's Weigert's
227 solution for 20 min, crocein scarlet acid / fuchsin solution for 1 min, 5 % phosphotungstic acid
228 for 5 min and 1 % acetic acid for 5 min. Between every staining step the tissue sections were

229 washed with tap water and distilled water. Sections were then covered with cytoseal mounting
230 medium. Every 15th section (~90 µm) of the brachiocephalic arteries and aortic roots were
231 analysed to quantify the plaque area. For histological analysis images were captured with a
232 Keyence BZ-X810 fluorescence microscope (aortic root) and an Olympus Bx43-Microscope
233 (brachiocephalic arteries). The Image Pro Plus software (version 6.0) software was used for
234 image analysis[14, 15, 17].
235 Cryosections were used for picrosirius red staining (Sigma-Aldrich, Germany) according to the
236 manufacturer's instructions. Tissue section were then stained with picrosirius red solution for
237 1 h at room temperature. Sections were then washed 2 times- in acidified water (5 ml glacial
238 acetic acid to 1 liter of water) and mounted. For histological analysis, images were captured
239 on a Keyence BZ-X810 fluorescence microscope and ImageJ software was used.
240
241 **Immunohistochemistry and immunofluorescence staining**
242 For immunohistochemistry and immunofluorescence staining, frozen sections of
243 brachiocephalic arteries or aortic roots were fixed in ice cold acetone for 8 min, washed twice
244 with ice cold PBS and incubated in 2% BSA in PBST for 1 hr. Sections were then incubated for
245 overnight at 4°C with primary antibodies against α-SMA (smooth muscle cells marker) and CD68
246 (macrophages markers). Sections incubated without primary antibodies were used as negative
247 controls for background correction. After overnight incubation the sections were washed three
248 times with PBS followed by incubation with corresponding horseradish peroxidase (HRP)-
249 labelled secondary antibodies. After washing, tissues were counterstained using 3,3'-
250 diaminobenzidine (DAB)/haematoxylin. Images were visualized, captured, and analysed using
251 a Keyence BZ-X810 all-in-one fluorescence microscope and an Olympus Bx43-Microscope
252 (Olympus, Hamburg, Germany). The Image J software (Version 1.8.0.) was used for image
253 analysis. Primary antibody against MOMA-2 (1:50, macrophages marker) was incubated for
254 overnight at 4°C followed by washing three times with PBS and incubation with fluorescently
255 labelled corresponding secondary antibody. Sections incubated without secondary antibody
256 were used as negative controls and for background correction. After washing, nuclear
257 counterstaining was conducted using mounting medium with DAPI. Images were visualized,
258 captured, and analysed using a fluorescence microscope (Keyence BZ-X810 and Olympus
259 Bx43-Microscope) using the same settings in experimental and control groups. Analyses were
260 performed by two independent blinded investigators. Image J software was used for image
261 analysis.
262
263 **Immunoblotting**
264 Proteins were isolated and immunoblotting was performed as described[18]. Mouse livers were
265 weighted and adjusted volume of RIPA buffer containing protease inhibitor cocktail (100 µl/10

266 mg) was added. Tissue was homogenized mechanically using 20G and 25G needles followed
267 by a 30 min incubation on ice with sequential vortexing. Samples were centrifuged at 12,000 x
268 g for 20 min at 4° C. Supernatant was transferred to a fresh tube and protein concentration was
269 determined using the Pierce™ BCA Protein Assay Kit following manufacturer's instructions and
270 Varioskan Lux plate reader (Thermo Fisher Scientific, Waltham, MA, USA). Samples were
271 separated using the Mini-PROTEAN® TGX™ Precast Gel 4-15% (Bio-Rad Laboratories, Inc.,
272 Hercules CA, USA) and transferred to a Nitrocellulose membrane. Membranes were incubated
273 with Invitrogen No-Stain solution for 10 min and blocked for 1 h in 5 % low-fat milk dissolved in
274 TBS-T. Incubation with primary anti-mLDLR antibody and anti-β-actin was performed overnight
275 at 4° C. Membranes were incubated with the corresponding secondary rabbit anti-goat
276 Immunoglobulins/HRP and Goat Anti-Mouse Immunoglobulins/HRP for 1 h at room
277 temperature. Millipore Immobilon Classico Western HRP Substrate was applied to detect the
278 signal using iBright 1500 (Thermo Fisher Scientific, Waltham, MA, USA). Densiometric analysis
279 was performed using ImageJ software.
280
281 **RNA-seq, functional annotation and pathway analysis**
282 RNA was extracted from aortic tissues (comprising the plaque and surrounding tissue) using
283 an RNeasy mini kit (QIAGEN, Germany), and RNA concentration was measured using a
284 nanodrop (2000C, Peq lab, Germany). The quality and integrity of RNA were controlled with
285 an Agilent Technologies 2100 Bioanalyzer (Agilent Technologies, Waldbronn, Germany).
286 Expression profiling was performed using RNA sequencing (RNA-seq). RNA sequencing
287 library was generated from 500 ng total RNA using Dynabeads® mRNA DIRECT(tm) Micro
288 Purification Kit (Thermo Fisher) for mRNA purification followed by NEBNext® Ultra(tm) II
289 Directional RNA Library Prep Kit (New England BioLabs) according to manufacturer's
290 protocols. The libraries were sequenced on Illumina NovaSeq 6000 using NovaSeq 6000 S2
291 Reagent Kit (100 cycles, paired end run) with an average of 3 x 10^7 reads per RNA sample. A
292 quality report is generated by the FASTQC (version 0.11.8) tool for each FASTQ file. Before
293 alignment to the reference genome, each sequence in the raw FASTQ files was trimmed on
294 base call quality and sequencing adapter contamination using the Trim Galore! wrapper tool
295 (version 0.4.4). Reads shorter than 20 bp were removed from the FASTQ file. Trimmed reads
296 were aligned to the reference genome using the open source short read aligner STAR (version
297 2.5.2b, https://code.google.com/p/rna-star/) with settings according to the log file. Feature
298 counts were determined using the R package Rsubread (version 1.32.4). Only genes showing
299 counts greater than 5 at least two times across all samples were considered for further analysis
300 (data cleansing). Gene annotation was performed using the R package bioMaRt (version
301 2.38.0). Before starting the statistical analysis steps, expression data were log2 transformed
302 and normalized according to the 50th percentile (quartile normalization using edgeR, version

303 3.24.3). Differential gene expression was calculated by the R package edgeR. Statistically
304 significant DEGs (p<0.05 and FDR <0.05) were sorted and categorized after correcting for
305 multiple hypothesis testing by Benjamini-Hochberg method. The threshold to identify
306 differentially expressed genes (DEGs) was set to a logFc value of ± 0.58 (IRI group), resulting
307 in a 1.5-fold expression change. To identify genes differentially regulated by either
308 hyperlipidemia (HCi) or combined hyperglycemia and hyperlipidemia (HGHCi), DEGs between
309 HFD (control) group and either group were identified based on a minimum logFc difference
310 value of ±0.58. Heatmapper (http://www.heatmapper.ca/) was used to generate heatmaps of
311 gene expression data. Genes shown in the heatmap were sorted based on DEGs in the control
312 group (HFD without PCSK9 injections) based on their log Fc values. For representation
313 purpose, no clustering method was applied and z-score was used. Venny (version 2.1), an
314 online interactive tool was used for comparison and identification of overlapping DEGs
315 between different groups. Gene ontology was performed using online tool, Database for
316 Annotation, Visualization and Integrated Discovery (DAVID) version 6.8 bioinformatics
317 package and Benjamini Hochberg adjustment was applied to all enriched p-values to control
318 for multiple testing. All RNAseq analyses were done by an independent blinded investigator.
319
320 **Statistical Analysis**
321 Statistical analyses were performed with Graph Pad Prism (version 7; Graph Pad Software
322 Inc., La Jolla, CA, USA). The significance level was set at p< 0.05 for all comparisons. The
323 data are summarized as mean ± standard error of the mean (SEM). Comparison of two groups
324 were analyzed with unpaired Student´s T-test. Statistical analyses of more than two groups
325 were performed with analysis of variance (ANOVA), and Sidak´s post hoc comparisons. The
326 Kolmogorov-Smirnov test or D'Agostino-Pearson normality test was used to determine
327 whether the data are consistent with Gaussian distribution.
328
329 **Results**
330
331 **Combination of hyperglycemia and hyperlipidemia exacerbates atherosclerosis in**
332 **PCSK9^{D377Y} expressing mice on a high-fat diet**
333 To induce hypercholesterolemia (HCi), 8 weeks old C57BL/6N mice were administrated a
334 single dose of rAAV8-PCSK9^{D377Y} (1.0 x 10^{11} adeno-associated viral particles, intravenously)
335 one week before feeding a high fat diet (HFD, Western type diet). Saline-injected mice fed a
336 HFD served as control for the rAAV8-PCSK9^{D377Y} intervention. Saline-injected mice with
337 genetic deficiency of low density lipoprotein receptor (LDLR$^{-/-}$) on HFD served as control for
338 rAAV8-PCSK9^{D377Y} treatment (**Figure 1A**). The mice group in which hypercholesterolemia
339 evoked by PCSK9-expression and HFD (HCi, single hit) was combined with induction of

340 chronic hyperglycemia using STZ-injection (double hit) is hereon termed as HGHCi (high
341 glucose high cholesterol - inducible) throughout the manuscript. For quantification of
342 atherosclerotic plaque formation mice were euthanized 12 (early timepoint) or 20 (late
343 timepoint) weeks after rAAV8-PCSK9^{D377Y} injection and start of HFD feeding.
344 As anticipated, rAAV8-PCSK9^{D377Y} administration, resulted in strong reduction of hepatic LDL
345 receptor protein levels as compared with saline injected mice both after 12 and 20 weeks of
346 intervention (**Figure 1B, C**). All mice thrived well and body weight (**Supplementary Table 1**),
347 blood lipids and glucose levels differed among treatment groups (**Figure 1D-F**). Plasma
348 cholesterol levels were higher in HGHCi group as compared to HCi animals both at early and
349 late timepoint analysis (**Figure 1D**), however, plasma triglyceride levels were higher in the
350 HGHCi vs HCi group only after 20 weeks (**Figure 1E**). Plasma triglyceride, cholesterol and
351 glucose levels were comparable between rAAV8-PCSK9^{D377Y} (HCi group) and LDLR$^{-/-}$ mice on
352 HFD (**Figure 1D-F**).
353 Analyses of haematoxylin and eosin (H&E) and Oil-Red O stained aortic root sections showed
354 larger atherosclerotic plaques in HGHCi mice compared to HCi mice, both at early and late
355 timepoint analysis (**Figure 2A-D**). Control mice had no lesions, whereas all rAAV8-
356 PCSK9^{D377Y}-injected mice on HFD (HCi group) developed atherosclerosis to a similar extent
357 like LDLR$^{-/-}$ mice on HFD (**Supplementary Figure II, A-H**). In addition, HGHCi mice on HFD
358 had larger plaques than LDLR$^{-/-}$ mice. Likewise, atherosclerotic plaques within the truncus
359 brachiocephalic artery were significantly larger in HGHCi mice compared to HCi mice at both
360 study time points (**Figure 2E, F**).
361
362 **Less stable plaque phenotypes in hyperglycemia and hyperlipidemia (HGHCi) *versus***
363 **hyperlipidemic (HCi) mice**
364 In addition to plaque size, plaque stability is an important determinant of clinical outcome. We
365 therefore evaluated parameters of plaque stability, in HCi and HGHCi mice. Indeed, signs of
366 plaque instability were more pronounced in HGHCi mice than in HCi mice as evident from an
367 increased necrotic core area and thinner fibrous caps of HGHCi mice (**Figure 2G- I**). Plaque
368 morphology and stability depend in part on the cellular composition of plaques. Smooth muscle
369 cells decreased within plaques of HGHCi mice after 20 weeks compared to HCi mice (**Figure**
370 **3A, B**). The content of macrophages, that were identified immunohistochemically by MOMA-2
371 staining was increased in plaques of truncus brachiocephalic artery (**Figure 3C**) of HGHCi
372 mice in comparison to HCi mice, both after 12 and 20 weeks. Taken together the observed
373 shift to increased macrophage and reduced SMC and collagen content indicates that plaque
374 stability is reduced in HGHCi mice[19, 20].
375
376

377 **Identification of HGHCi-specific transcriptional responses in the aorta**
378 We next aimed to identify transcriptional signatures that are engaged in the vasculature by
379 combined chronic hyperlipidemia and hyperglycemia to generate hypotheses about signaling
380 pathways contributing to larger but unstable plaques in HGHCi mice. To this end we conducted
381 unbiased gene expression analyses (RNAseq) in the cohorts of control, HCi and HGHCi mice
382 at 12 weeks. In aortic tissue of HCi mice, the expression of 942 genes was induced compared
383 to controls from mice solely on a HFD (**Figure 4A**). Conversely, gene expression in the aorta
384 of HGHCi mice was strikingly different from that of HCi mice. Gene expression of a large set
385 of genes was dysregulated in HGHCi mice. Thus, in aortic tissue of HGHCi mice, the
386 expression of 2759 genes was induced compared to aortic samples of saline treated HFD fed
387 mice (**Figure 4A**). 418 genes showed similar expression in both HGHCi and HCi mice, a
388 differential regulation of 2341 genes could be specifically assigned to combined hyperglycemia
389 and hyperlipidemia.
390 We next performed functional annotation analysis to study the gene pathways that are
391 specifically engaged in the vessels of the HGHCi group, and observed that combined
392 hyperglycemia plus hyperlipidemia lead to significant changes in the expression of genes
393 encoding signaling molecules involved in inflammation, intracellular lipid transport, cholesterol
394 metabolic processes, collagen degradation, and cellular metabolism (**Figure 4B**). We further
395 performed gene ontology analysis on genes that were induced in aortic tissue of HCi and
396 HGHCi mice. Gene ontology analysis of differentially expressed genes revealed that combined
397 hyperglycemia and hyperlipidemia leads to upregulation of genes involved in inflammatory
398 response and collagen degradation (**Figure 4C, D**).
399
400 **Paigen diet accentuates atherosclerosis and promotes plaque instability in mice with**
401 **combined hyperglycemia and hyperlipidemia on paigen diet**
402 We next tested the atherosclerosis model following induction of combined hyperglycemia and
403 hyperlipidemima (HGHCi) in mice fed with a Paigen diet (PD), which leads to higher plasma
404 cholesterol levels [7] and, thus, might further accelerate the formation of atherosclerotic
405 plaques. PD fed mice were treated with the same batch and dose of rAAV8-PCSK9^{D377Y}, and
406 LDLR$^{-/-}$mice on PD served as reference for the comparison, saline-injected mice fed on PD
407 served as control for the rAAV8-PCSK9^{D377Y} intervention. Hyperlipidemic and hyperlipidemic
408 plus hyperglycemic mice on PD are for simplicity hereafter called as HCi- PD and HGHCi- PD
409 mice, respectively. In HGHCi- PD mice, we observed an increased mortality (25% in week 8,
410 i.e. 5 out of 20 mice died in this group) (**Supplementary Figure I, A**). Based on these
411 incidences, it was decided that the remaining animals in this group should be sacrificed and
412 analysed already 8- 9 weeks after induction of combined hypercholesterolemia and
413 hyperglycemia, since the 12 and 20 weeks time points chosen for the HGHCi group on HFD

414 might not have been reached. Thus, mice from all groups on the PD diet were euthanized 8-9
415 weeks after rAAV8-PCSK9^{D377Y} injection to quantify atherosclerosis (**Figure 5A**). Hepatic LDL
416 receptor protein expression was already abrogated at this time point as compared with saline
417 injected mice (control) (**Figure 5B, C**). As expected, body weight (**Supplementary Table 1)**,
418 plasma cholesterol levels and blood glucose levels differed among treatment groups (**Figure**
419 **5D-F).** In a preliminary pilot study, we compared plasma cholesterol levels of a HGHCi-PD
420 group with STZ-treated mice (STZ-PD) and citrate-treated controls (citrate-PD) fed with Paigen
421 diet, respectively (**Supplementary Figure 4**). Notably, mice with STZ-evoked hyperglycemia
422 and on a high-cholesterol, high-fat Paigen diet (without AAV-mPCSK9 treatment) did not
423 exhibit an increase in plasma cholesterol (**Supplementary Figure 4).** Application of the Paigen
424 diet accelerated atherosclerosis in both HGHCi-PD and HCi-PD mice compared to
425 corresponding groups on HFD diet ($p < 0.05$). Interestingly, aortic root plaque sizes of HGHCi-
426 PD and HCi-PD mice at 8 weeks (**Figure 5G-J)** were comparable to HGHCi and HCi mice on
427 HFD at 20 weeks, respectively (**Figure 2A**). Consistent with data from the HFD diet groups,
428 signs of plaque instability were more pronounced in HGHCi-PD mice than in HCi-PD mice as
429 measured by decreased collagen deposition (picro sirus red staining) and increased plaque
430 macrophages content (CD68-positive cells) in plaques of HGHCi-PD mice in comparison with
431 HCi-PD mice (**Figure 6A-D**). Taken together these data suggest that PD accelerates
432 atherosclerosis in mice and shows plaque formation already after 8 weeks, therefore,
433 representing a fast and direct inducible diabetic atherosclerosis model.
434

435 **Discussion**

436 The most frequently used models to study diabetes mellitus associated accelerated
437 atherosclerosis in mice are relying on genetically modified models. Thus, mouse studies
438 evaluating diabetes-associated atherosclerosis rely on ApoE$^{-/-}$ or LDLR$^{-/-}$ mice, where
439 hypercholesterolemia is combined with chronic hyperglycemia following beta cell destruction
440 by injection of streptozotocin (STZ) or viral infection[21] or by cross-breeding with mouse
441 strains carrying a point mutation in the gene encoding insulin leading to a misfolding of the
442 proinsulin 2 protein (Ins2^{+}/Akita)[4, 22]. Induction of hyperglycemia with STZ lead to higher
443 plasma cholesterol levels and show significant acceleration of atherosclerotic lesion formation
444 in ApoE$^{-/-}$ and LDLR$^{-/-}$ mice compared to non-diabetic ApoE$^{-/-}$ and LDLR$^{-/-}$ controls[6, 23–29].
445 Also the severe hyperglycemia in Ins2^{+}/Akita mice cross-bred with ApoE$^{-/-}$ and LDLR$^{-/-}$ leads
446 to a pronounced increase in atherosclerosis and non-HDL cholesterol and triglyceride levels
447 compared to non-hyperglycemic control mice[4, 30, 31]. Although these genetic models are
448 useful tools for studying diabetic complications, it requires intensive cross-breading of these
449 mouse lines. This becomes even more laborious and time consuming when diabetic long-term
450 complications are to be induced in knockout mouse lines for evaluation of the causal role of

451 the gene of interest under certain metabolic conditions. Concomitant induction of both
452 hypercholesterolemia and hyperglycemia at discrete time points in a given mouse line has not
453 been reported.
454 Here, we describe a novel strategy to induce an atherosclerosis model aggravated by
455 concomitant induction of hyperglycemia without the necessity of genetic germline engineering
456 but via rAAV8-mediated gene transfer of mutant PCSK9^{D377Y} in hepatocytes in combination
457 with STZ-evoked beta cell destruction (HGHCi). Comparison of plasma cholesterol levels
458 shows increased cholersterol levels in the HCi model, which increase further by additional
459 induction of hyperglycemia in the HGHCi model. The additional increase in cholesterol levels
460 is a consequence of the two-hit model, because induction of hyperglycemia alone does not
461 increase plasma cholesterol levels. The increased plasma cholesterol levels in the diabetic
462 mice (HGHCi group) are part of the phenotype of our model and resemble findings in previous
463 studies[7,26,29,28]. Dyslipidaemia aggravated by hyperglycaemia is independent of whether the
464 diabetes was induced by STZ injection or genetically (e.g., InsAkita mutant mice). Increased
465 cholesterol levels in the diabetic mice most likely reflect decreased lipoprotein clearance and
466 as such may reflect an important feature of diabetes associated dyslipidaemia. Thus, Goldberg
467 et al. demonstrated that plasma cholesterol levels of STZ- induced diabetic LDLR$^{-/-}$ mice were
468 twice those of nondiabetic control mice. The authors observed an increase in both VLDL and
469 LDL. VLDL in plasma was more enriched in cholesterol, and both VLDL and LDL had higher
470 levels of ApoE [29]. Further lipidomics analyses are required to define the lipid profile in
471 diabetic and non-diabetic mice with PCSK9^{D377Y} induced dyslipidaemia. Furthermore, we show
472 that combined hyperlipidemia and hyperglycemia lead to a significant acceleration and
473 enhancement of atherosclerotic plaque formation compared to mice in which
474 hypercholesterolemia was induced without hyperglycemia (HCi). The HCi model in rAAV8-
475 mediated mutant PCSK9^{D377Y} expressing mice leads to down-regulation of hepatic LDL
476 receptor expression and the development of atherosclerotic lesions. The lesion phenotypes
477 closely resemble those in the established LDL-receptor knockout mouse model. Mice of the
478 HGHCi treatment group displayed larger plaques compared to norrmoglycemic HCi mice on
479 the same diet. The treatment induced systemic atherosclerosis, e.g. in the aortic roots and in
480 the brachiocephalic artery. The plaque phenotypes induced by HGHCi compared to HCi mice
481 are characterized by increased necrotic core area, decreased fibrous cap thickness and
482 increased frequency of rupture shoulder. Plaques are characterized by increased
483 macrophages and reduced smooth muscle cell content. These data show that the novel HGHCi
484 model provides the prerequisites to study interventions aiming to improve plaque size and –
485 importantly - plaque stability.
486 Similar severity of atherosclerosis was observed on Paigen fed diet albeit much earlier, 8
487 weeks post intervention initiation, compared to 20 weeks on HFD. It is reported that the addition

488 of cholate in combination with high-cholesterol and high-fat content in Paigen diet boost
489 hypercholesterolemia by facilitating fat and cholesterol absorption resulting in very early fatty
490 streak lesions in the aortic root and proximal aorta in C57BL/6 mice[32]. Thus, our findings are
491 in line with previous work in genetic models, demonstrating that hyperglycemia promotes
492 unstable plaques in both ApoE$^{-/-}$ or LDLR$^{-/-}$ mice[14, 33–35]. Our results identify the HGHCi-
493 PD model using Paigen diet as novel option for specific experimental set-ups where a very
494 rapid induction of atherosclerosis is needed.
495 Our unbiased gene expression analysis revealed that combined hyperlipidemia and
496 hyperglycemia (HGHCi) dysregulates a large set of genes (i.e. 2341 genes) in the
497 atherosclerotic aorta compared to hyperlipidemia alone (HCi). The aortic tissue gene
498 expression profile of HGHCi mice fed a HFD differed markedly from HCi mice. Among the
499 pathways that were most prominently affected were inflammation, metabolism and particularly
500 immunometabolism, and collagen degradation.
501 These findings are reminiscent to previous studies, demonstrating that dysregulated
502 immunometabolism promotes diabetes-associated acceleration of atherosclerosis[33, 36]. The
503 increased expression of genes related to collagen degradation is consistent with previous
504 finding showing glucose-induced advanced glycation end products (RAGE) mediate
505 modification of the components of the extracellular matrix and accelerates atherosclerosis
506 under diabetic conditions[37–40]. The expression data may provide a helpful resource for
507 researchers using this model and suggest that this non-genetic model will be suitable to study
508 important aspects of the emerging cross-talk between inflammatory signalling, glucose- and
509 lipoprotein metabolism[22, 41–43].
510 The study has some limitations. The aim of the study was to develop and to characterize novel
511 models of hyperlipidemia and hyperglycemic associated atherosclerosis. Plasma lipid levels
512 were not identical between groups. Due to the study design, a cohort with only STZ injection
513 was not included as hyperglycemia induced by STZ treatment or lymphocytic choriomeningitis
514 virus (LCMV) infection alone is not sufficient to induce atherosclerosis development in mice[28,
515 33]. Hence, conclusion about an impact of isolated hyperglycaemia atherosclerotic plaque
516 phenotype cannot be drawn from the current study.
517
518 **Conclusion**
519 We describe a novel non-genetic inducible mouse model using a defined treatment with gain-
520 of-function PCSK9 viral particles, streptozotocin and high-fat diets. The detailed
521 characterization of the plaques phenotypes and the expression analysis indicate that this new
522 experimental approach can be used to study the clinically important pathogenesis of
523 atherosclerosis in hyperglycemia and hyperlipidemia, and can be induced at any given time

point to prevent or to therapeutically interfere with the development of atherosclerosis under diabetic conditions.

Acknowledgement

We thank Sonja Talmon, Beate Hilbert, Christin Richter, Manuela Ritzal, Anja Barnikol-Oettler, and Kathrin Deneser for excellent technical support. We certify that all persons who have made substantial contributions to the manuscript, but who do not fulfill authorship criteria, are named in the acknowledgments section and have provided the corresponding author with written permission to be named in the manuscript.

Authors Contribution:

S.G., K.S. and R.M., interpreted the experimental work and prepared the manuscript. A.W., R.M., S.G., I.G. and D.S. performed and conducted the *in vivo* experiments; S.G., I.G., and C.M., performed histological analyses and figure preparation; J.H., J.B., and H.K. performed RNAseq analysis; S.A. and S.F. assisted in histology. B.I. and U. L. interpreted the data and assisted in manuscript preparation. M.F. designed the study and assisted in manuscript preparation.

Sources of Funding

This work was supported by grants of the 'Deutsche Forschungsgemeinschaft' (including project S03 of the Collaborative Research Centers (SFB) SFB1118 (MF), and IS-67/5-3, IS-67/8-1, IS-67/11-1, and CRC854/B26 to B.I., SH 849/4-1 to K.S.

Disclosures

The authors have nothing to disclose.

References

[1] Correction to: Heart Disease and Stroke Statistics-2019 Update: A Report From the American Heart Association. Circulation 2020;141(2):e33.

[2] Raghavan S, Vassy JL, Ho Y-L, Song RJ, Gagnon DR, Cho K et al. Diabetes Mellitus-Related All-Cause and Cardiovascular Mortality in a National Cohort of Adults. Journal of the American Heart Association 2019;8(4):e011295.

[3] Fang M, Wang D, Coresh J, Selvin E. Trends in Diabetes Treatment and Control in U.S. Adults, 1999–2018. The New England journal of medicine 2021;384(23):2219–28.

558 [4] Jun JY, Ma Z, Segar L. Spontaneously diabetic Ins2+/Akita:apoE-deficient mice exhibit
559 exaggerated hypercholesterolemia and atherosclerosis. American Journal of Physiology-
560 Endocrinology and Metabolism 2011;301(1):E145-E154.
561 [5] Voyiaziakis E, Goldberg IJ, Plump AS, Rubin EM, Breslow JL, Huang LS. ApoA-I
562 deficiency causes both hypertriglyceridemia and increased atherosclerosis in human
563 apoB transgenic mice. Journal of lipid research 1998;39(2):313–21.
564 [6] Keren P, George J, Keren G, Harats D. Non-obese diabetic (NOD) mice exhibit an
565 increased cellular immune response to glycated-LDL but are resistant to high fat diet
566 induced atherosclerosis. Atherosclerosis 2001;157(2):285–92.
567 [7] Bjorklund MM, Hollensen AK, Hagensen MK, Dagnaes-Hansen F, Christoffersen C,
568 Mikkelsen JG et al. Induction of atherosclerosis in mice and hamsters without germline
569 genetic engineering. Circulation research 2014;114(11):1684–9.
570 [8] Goettsch C, Hutcheson JD, Hagita S, Rogers MA, Creager MD, Pham T et al. A single
571 injection of gain-of-function mutant PCSK9 adeno-associated virus vector induces
572 cardiovascular calcification in mice with no genetic modification. Atherosclerosis
573 2016;251:109–18.
574 [9] Grieger JC, Choi VW, Samulski RJ. Production and characterization of adeno-associated
575 viral vectors. Nature protocols 2006;1(3):1412–28.
576 [10] Zolotukhin S, Byrne BJ, Mason E, Zolotukhin I, Potter M, Chesnut K et al. Recombinant
577 adeno-associated virus purification using novel methods improves infectious titer and
578 yield. Gene Therapy 1999;6(6):973–85.
579 [11] Jungmann A, Leuchs B, Rommelaere J, Katus HA, Müller OJ. Protocol for Efficient
580 Generation and Characterization of Adeno-Associated Viral Vectors. Human gene
581 therapy methods 2017;28(5):235–46.
582 [12] Ishibashi S, Goldstein JL, Brown MS, Herz J, Burns DK. Massive xanthomatosis and
583 atherosclerosis in cholesterol-fed low density lipoprotein receptor-negative mice. The
584 Journal of clinical investigation 1994;93(5):1885–93.
585 [13] Zhou Q, Bea F, Preusch M, Wang H, Isermann B, Shahzad K et al. Evaluation of Plaque
586 Stability of Advanced Atherosclerotic Lesions in Apo E-Deficient Mice after Treatment with
587 the Oral Factor Xa Inhibitor Rivaroxaban. Mediators of Inflammation 2011;2011:432080.
588 [14] Shahzad K, Gadi I, Nazir S, Al-Dabet M'dM, Kohli S, Bock F et al. Activated protein C
589 reverses epigenetically sustained $p66^{Shc}$ expression in plaque-associated macrophages
590 in diabetes. Communications biology 2018;1:104.
591 [15] Seehaus S, Shahzad K, Kashif M, Vinnikov IA, Schiller M, Wang H et al.
592 Hypercoagulability inhibits monocyte transendothelial migration through protease-
593 activated receptor-1-, phospholipase-Cbeta-, phosphoinositide 3-kinase-, and nitric oxide-

594 dependent signaling in monocytes and promotes plaque stability. Circulation
595 2009;120(9):774–84.
596 [16] Shahzad K, Thati M, Wang H, Kashif M, Wolter J, Ranjan S et al. Minocycline reduces
597 plaque size in diet induced atherosclerosis via p27(Kip1). Atherosclerosis
598 2011;219(1):74–83.
599 [17] Schuster S, Rubil S, Endres M, Princen HMG, Boeckel J-N, Winter K et al. Anti-PCSK9
600 antibodies inhibit pro-atherogenic mechanisms in APOE*3Leiden.CETP mice. Scientific
601 reports 2019;9(1):11079.
602 [18] Gaul S, Leszczynska A, Alegre F, Kaufmann B, Johnson CD, Adams LA et al. Hepatocyte
603 pyroptosis and release of inflammasome particles induce stellate cell activation and liver
604 fibrosis. Journal of Hepatology.
605 [19] Harman JL, Jørgensen HF. The role of smooth muscle cells in plaque stability:
606 Therapeutic targeting potential. British journal of pharmacology 2019;176(19):3741–53.
607 [20] Doran AC, Meller N, McNamara CA. Role of smooth muscle cells in the initiation and early
608 progression of atherosclerosis. Arteriosclerosis, thrombosis, and vascular biology
609 2008;28(5):812–9.
610 [21] SHEN XIA, BORNFELDT KE. Mouse Models for Studies of Cardiovascular Complications
611 of Type 1 Diabetes. Annals of the New York Academy of Sciences 2007;1103(1):202–17.
612 [22] Oppi S, Lüscher TF, Stein S. Mouse Models for Atherosclerosis Research—Which Is My
613 Line? Frontiers in Cardiovascular Medicine 2019;6:46.
614 [23] Tse J, Martin-McNaulty B, Halks-Miller M, Kauser K, DelVecchio V, Vergona R et al.
615 Accelerated atherosclerosis and premature calcified cartilaginous metaplasia in the aorta
616 of diabetic male Apo E knockout mice can be prevented by chronic treatment with 17β-
617 estradiol. Atherosclerosis 1999;144(2):303–13.
618 [24] Vikramadithyan RK, Hu Y, Noh H-L, Liang C-P, Hallam K, Tall AR et al. Human aldose
619 reductase expression accelerates diabetic atherosclerosis in transgenic mice. The Journal
620 of clinical investigation 2005;115(9):2434–43.
621 [25] Lewis P, Stefanovic N, Pete J, Calkin AC, Giunti S, Thallas-Bonke V et al. Lack of the
622 Antioxidant Enzyme Glutathione Peroxidase-1 Accelerates Atherosclerosis in Diabetic
623 Apolipoprotein E–Deficient Mice. Circulation 2007;115(16):2178–87.
624 [26] Vedantham S, Noh H, Ananthakrishnan R, Son N, Hallam K, Hu Y et al. Human Aldose
625 Reductase Expression Accelerates Atherosclerosis in Diabetic Apolipoprotein E−/− Mice.
626 Arteriosclerosis, thrombosis, and vascular biology 2011;31(8):1805–13.
627 [27] Park L, Raman KG, Lee KJ, Lu Y, Ferran LJ, Chow WS et al. Suppression of accelerated
628 diabetic atherosclerosis by the soluble receptor for advanced glycation endproducts.
629 Nature Medicine 1998;4(9):1025–31.

630 [28] Hammad SM, Hazen-Martin DJ, Sohn M, Eldridge L, Powell-Braxton L, Won W et al.
631 Nephropathy in a Hypercholesterolemic Mouse Model with Streptozotocin-Induced
632 Diabetes. Kidney Blood Press Res 2003;26(5-6):351–61.
633 [29] Goldberg IJ, Hu Y, Noh H-L, Wei J, Huggins LA, Rackmill MG et al. Decreased lipoprotein
634 clearance is responsible for increased cholesterol in LDL receptor knockout mice with
635 streptozotocin-induced diabetes. Diabetes 2008;57(6):1674–82.
636 [30] Zhou C, Pridgen B, King N, Xu J, Breslow JL. Hyperglycemic Ins2AkitaLdlr−/− mice show
637 severely elevated lipid levels and increased atherosclerosis: a model of type 1 diabetic
638 macrovascular disease[S]. Journal of lipid research 2011;52(8):1483–93.
639 [31] Engelbertsen D, To F, Dunér P, Kotova O, Söderberg I, Alm R et al. Increased
640 Inflammation in Atherosclerotic Lesions of Diabetic *Akita-LDLr*$^{-/-}$ Mice Compared to
641 Nondiabetic *LDLr*$^{-/-}$ Mice. Experimental Diabetes Research 2012;2012:176162.
642 [32] Getz GS, Reardon CA. Diet and Murine Atherosclerosis. Arteriosclerosis, thrombosis, and
643 vascular biology 2006;26(2):242–9.
644 [33] Johansson F, Kramer F, Barnhart S, Kanter JE, Vaisar T, Merrill RD et al. Type 1 diabetes
645 promotes disruption of advanced atherosclerotic lesions in LDL receptor-deficient mice.
646 Proceedings of the National Academy of Sciences of the United States of America
647 2008;105(6):2082–7.
648 [34] BORNFELDT KE. Uncomplicating the Macrovascular Complications of Diabetes: The
649 2014 Edwin Bierman Award Lecture. Diabetes 2015;64(8):2689–97.
650 [35] Renard CB, Kramer F, Johansson F, Lamharzi N, Tannock LR, Herrath MG von et al.
651 Diabetes and diabetes-associated lipid abnormalities have distinct effects on initiation and
652 progression of atherosclerotic lesions. The Journal of clinical investigation
653 2004;114(5):659–68.
654 [36] Stitziel NO, Kanter JE, BORNFELDT KE. Emerging Targets for Cardiovascular Disease
655 Prevention in Diabetes. Trends in molecular medicine 2020;26(8):744–57.
656 [37] Ihara Y, Egashira K, Nakano K, Ohtani K, Kubo M, Koga J-i et al. Upregulation of the
657 ligand-RAGE pathway via the angiotensin II type I receptor is essential in the
658 pathogenesis of diabetic atherosclerosis. Journal of molecular and cellular cardiology
659 2007;43(4):455–64.
660 [38] Bu D-x, Rai V, Shen X, Rosario R, Lu Y, D'Agati V et al. Activation of the ROCK1 branch
661 of the transforming growth factor-beta pathway contributes to RAGE-dependent
662 acceleration of atherosclerosis in diabetic ApoE-null mice. Circulation research
663 2010;106(6):1040–51.
664 [39] Soro-Paavonen A, Watson AMD, Li J, Paavonen K, Koitka A, Calkin AC et al. Receptor
665 for advanced glycation end products (RAGE) deficiency attenuates the development of
666 atherosclerosis in diabetes. Diabetes 2008;57(9):2461–9.

667 [40] Wang Z, Jiang Y, Liu N, Ren L, Zhu Y, An Y et al. Advanced glycation end-product Nε-
668 carboxymethyl-Lysine accelerates progression of atherosclerotic calcification in diabetes.
669 Atherosclerosis 2012;221(2):387–96.
670 [41] Martins IJ, Hone E, Foster JK, Sünram-Lea SI, Gnjec A, Fuller SJ et al. Apolipoprotein E,
671 cholesterol metabolism, diabetes, and the convergence of risk factors for Alzheimer's
672 disease and cardiovascular disease. Molecular psychiatry 2006;11(8):721–36.
673 [42] Farmer BC, Johnson LA, Hanson AJ. Effects of apolipoprotein E on nutritional metabolism
674 in dementia. Current opinion in lipidology 2019;30(1):10–5.
675 [43] Hui DY, Basford JE. Distinct signaling mechanisms for apoE inhibition of cell migration
676 and proliferation. Neurobiology of aging 2005;26(3):317–23.

Figures

Figure 1

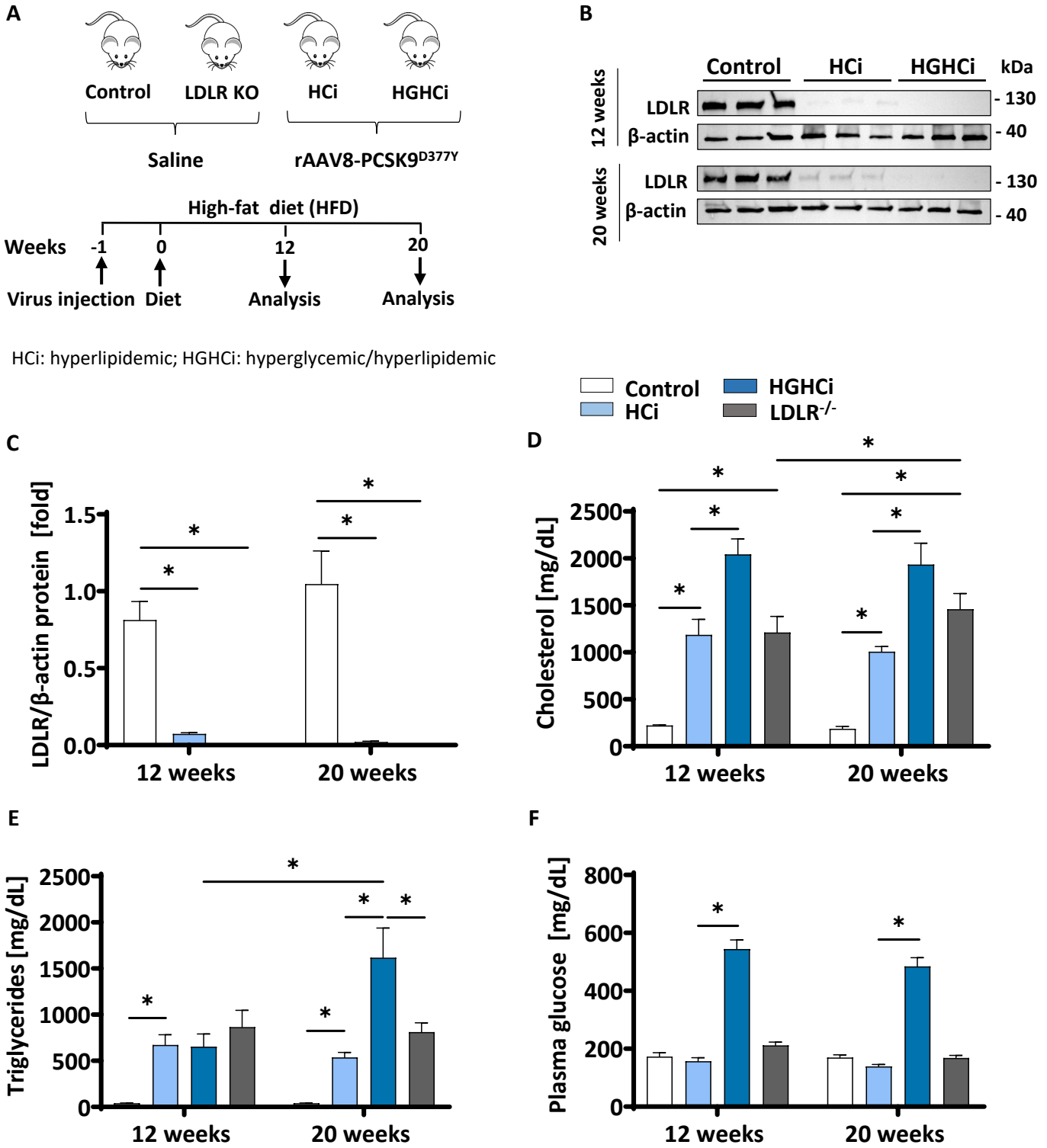

Figure 1: Simultaneous treatment of rAAV8-PCSK9 virus and Streptozotocin induces a hyperlipidemic and hyperglycemic mouse phenotype. A: Schematic summary of the experimental setup. Mice were analyzed after 12 or 20 weeks of interventions initiation. Wild type mice without rAAV8-PCSK9^{D377Y} injection on high-fat diet (HFD, 21 % fat, 0.21 % cholesterol) was used as control. Mice injected with rAAV8-PCSK9^{D377Y} and fed a HFD are termed HCi (hyperlipidemic), or injected with both rAAV8-PCSK9^{D377Y} and streptozotocin and fed a HFD are termed HGHCi (hyperlipidemic and hyperglycemic). LDLR-/- mice on HFD served as reference control. B: Representative immunoblot of liver lysate showing hepatic protein levels of low-density lipoprotein receptor (LDLR). β-actin was used as loading control. C: Densitometric analysis of LDLR immunoblot was normalized on β-actin and referred to control group which is set at 1. Bar graphs are showing level of D: plasma cholesterol level [mg/dL, E: Triglycerides [mg/dL] and F: blood glucose levels [mg/dL]. Data are presented as mean ± SEM and one-way ANOVA was performed with Sidak's multiple comparison post-hoc test (*$p < 0.05$). N= 6 for each group.

Figure 2

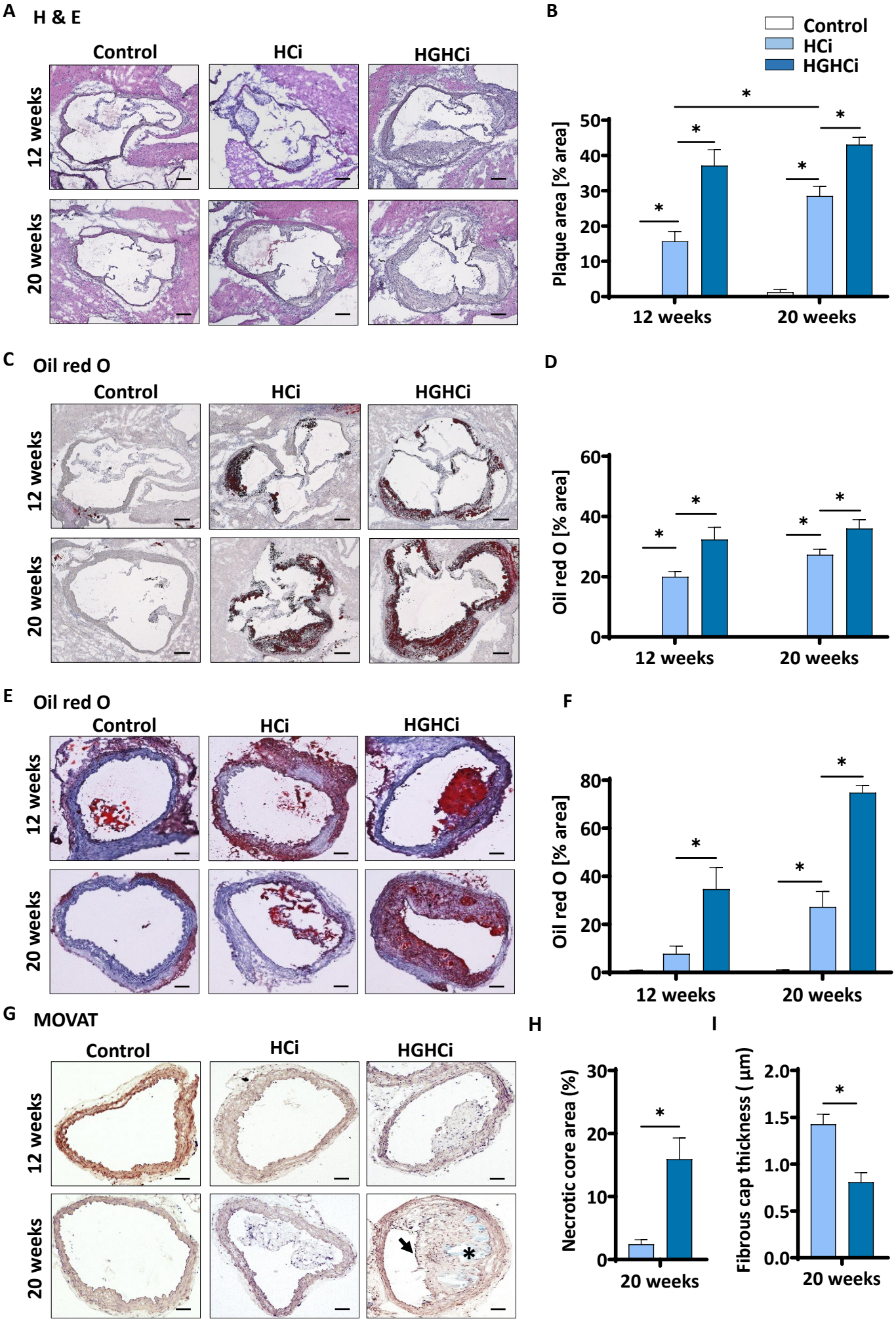
A
H & E
Control
HCi
HGHCi
12 weeks
20 weeks
B
Control
HCi
HGHCi
Plaque area [% area]
12 weeks
20 weeks
C
Oil red O
Control
HCi
HGHCi
12 weeks
20 weeks
D
Oil red O [% area]
12 weeks
20 weeks
E
Oil red O
Control
HCi
HGHCi
12 weeks
20 weeks
F
Oil red O [% area]
12 weeks
20 weeks
G
MOVAT
Control
HCi
HGHCi
12 weeks
20 weeks
H
Necrotic core area (%)
20 weeks
I
Fibrous cap thickness (µm)
20 weeks

Figure 2: Mice with combined hyperlipidemia and hyperglycemia show larger plaques than hyperlipidemic mice. A-D: Representative histological images showing aortic root sections stained with Hematoxylin/ Eosin (H & E, A) and bar graphs summarizing data (B). Representative histological images showing aortic root sections stained with Oil-Red O (C) and bar graphs summarizing data (D). E-H: Representative histological images showing truncus brachiocephalic arteries sections stained with Oil-Red O (E,) and bar graphs summarizing data (F). Representative images showing MOVATs pentachrome staining of truncus brachiocephalic arteries (G). Bar graphs summarizing morphometric analyses of MOVATs stained images for necrotic core area (H) and fibrous caps (I). Necrotic core area within plaque is indicated by*, fibrous caps thickness by a black arrow in MOVAT stained truncus brachiocephalic arteries (G, bottom panel) . Data presented as mean ± SEM and one-way ANOVA was performed with Sidak's multiple comparison post-hoc test (*$p < 0.05$). Stainings are imaged at 4 × magnification, scale bar 200 µm (A, C, E, G). HFD control 12 and 20 weeks (N= 7), HCi 12 and 20 weeks (N= 5), and HGHCi 12 and 20 weeks (N= 6).

Control: Wild type mice without rAAV8-PCSK9D377Y injection on high fat diet (HFD); HCi: rAAV8-PCSK9D377Y injection plus HFD (hyperlipidemic); HGHCi: rAAV8-PCSK9D377Y and streptozotocin injection and HFD (hyperlipidemic and hyperglycemic).

Figure 3

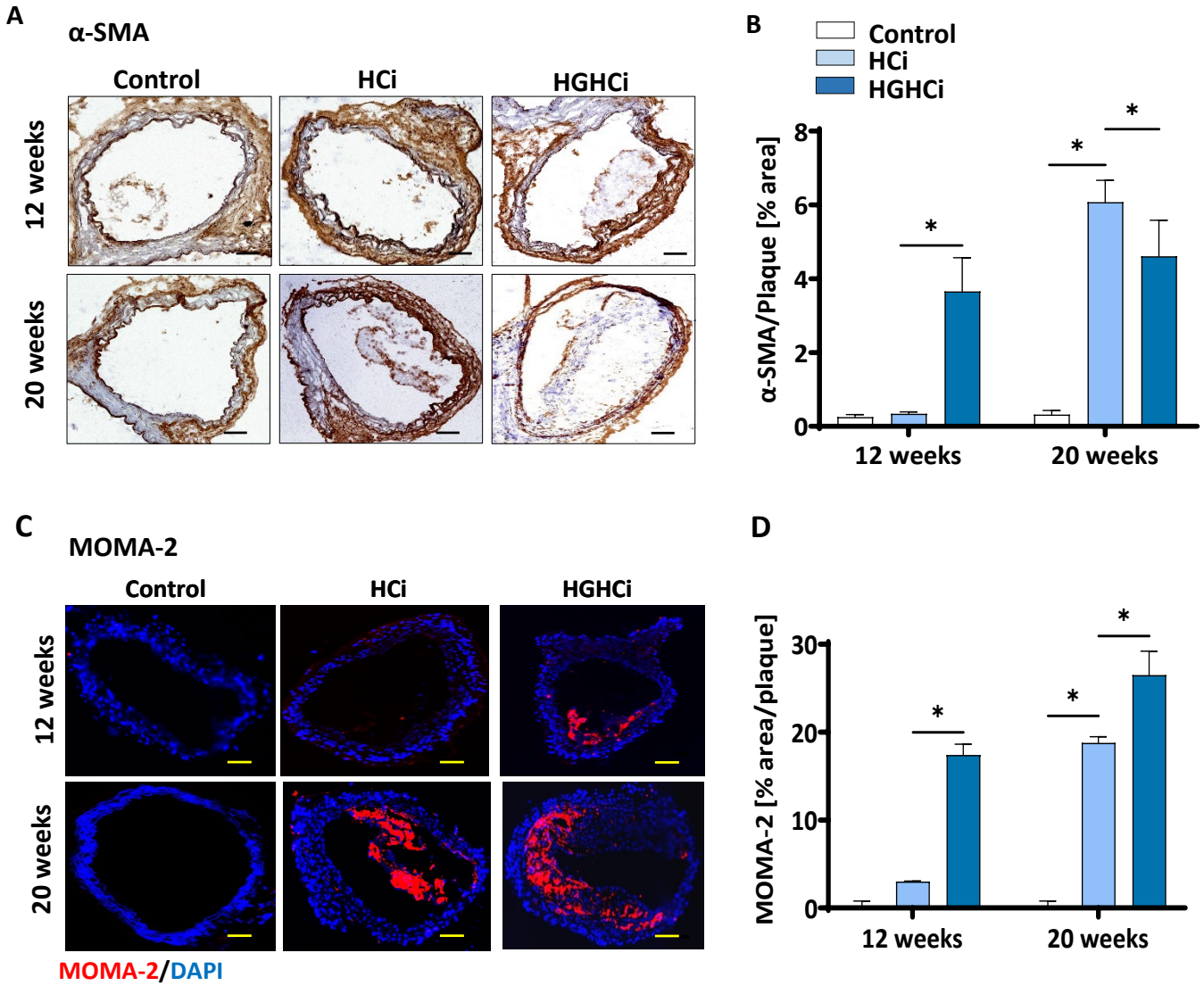
A
α-SMA
Control
HCi
HGHCi
12 weeks
20 weeks
B
Control
HCi
HGHCi
α-SMA/Plaque [% area]
0
2
4
6
8
*
12 weeks
20 weeks
C
MOMA-2
Control
HCi
HGHCi
12 weeks
20 weeks
MOMA-2/DAPI
D
MOMA-2 [% area/plaque]
0
10
20
30
*
12 weeks
20 weeks

Figure 3: Less smooth muscle cells and collagen content within plaques of hyperlipidemic and hyperglycemic mice as compared to hyperlipidemic mice. A, B: Representative images showing immunohistochemical staining for smooth muscle cell marker α-SMA (positive cells detected by HRP-DAB reaction, brown) on truncus brachiocephalic arteries sections (**A**, scale bar 200 µm) and bar graphs summarizing data (**B**). The data are presented as mean ± SEM and one-way ANOVA was performed with Sidak's multiple comparison post-hoc test (*$p < 0.05$). **C, D:** Representative images showing immunofluorescence staining of truncus brachiocephalic arteries sections for macrophages marker MOMA-2 (**C,** MOMA-2= red; DAPI nuclear counterstain= blue) and bar graphs summarizing data (**D**). The data are presented as mean ± SEM and one-way ANOVA was performed with Sidak's multiple comparison post-hoc test (*$p < 0.05$). Scale bar 200 µm. Control 12 and 20 weeks (N= 7), HCi 12 weeks (N= 5) and 20 weeks (N= 6), HGHCi 12 weeks (N= 7) and 20 weeks (N= 6). Control: Wild type mice without rAAV8-PCSK9^{D377Y} injection on high fat diet (HFD); HCi: rAAV8-PCSK9^{D377Y} injection plus HFD (hyperlipidemic); HGHCi: rAAV8-PCSK9^{D377Y} and streptozotocin injection and HFD (hyperlipidemic and hyperglycemic).

Figure 4

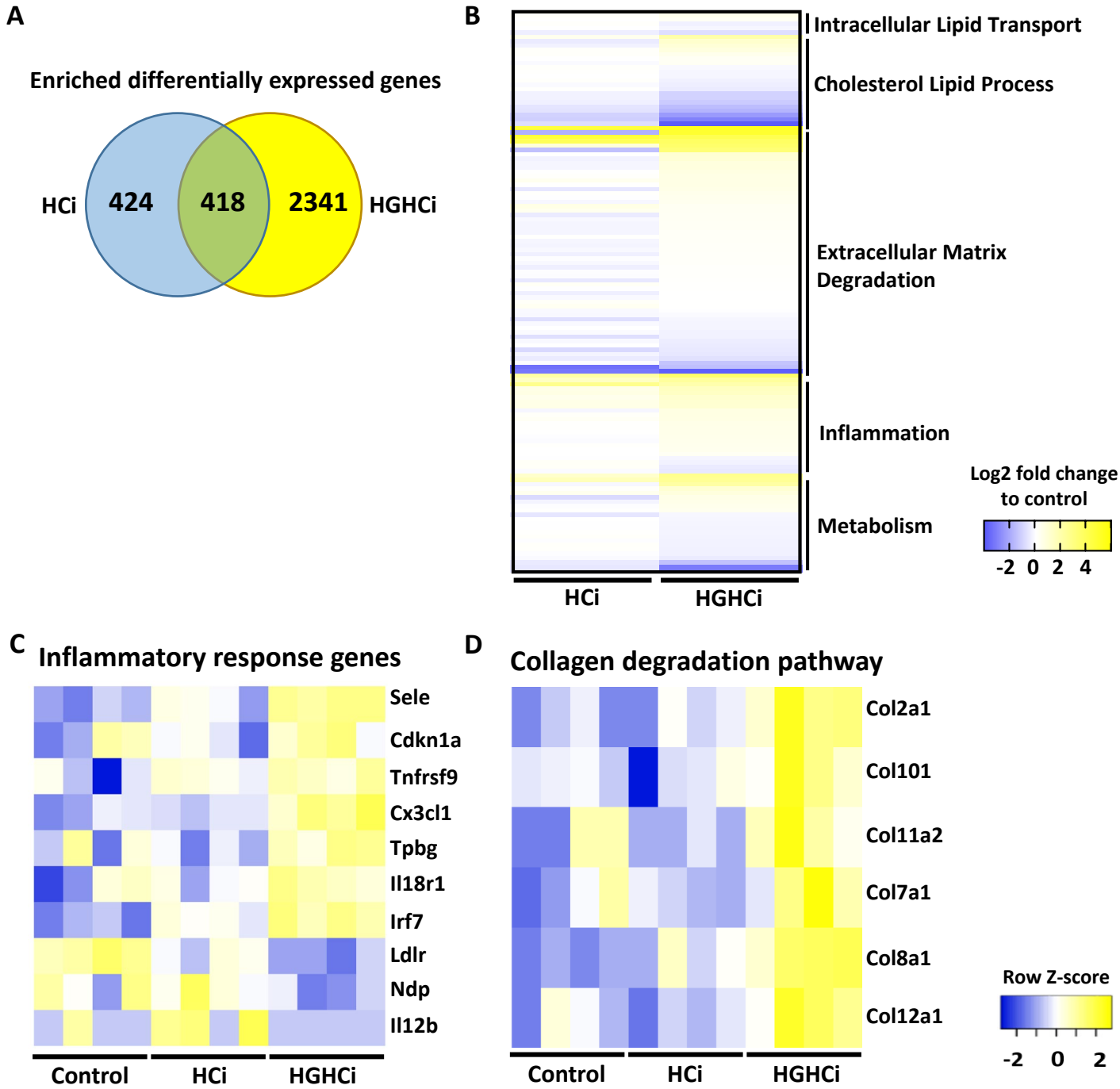

Figure 4: Combined hyperglycemia and hyperlipidemia induce large set of differentially expressed genes and activates inflammatory response and collagen degradation pathways. RNA sequencing in aortic tissue of control, HCi and HGHCi mice after 12 weeks. Wild type mice without AAV8-PCSK9^{D377Y} injection on high fat diet (control) or injected with rAAV8-PCSK9^{D377Y} and on HFD (hyperlipidemic, HCi) or injected with both rAAV8-PCSK9^{D377Y} and streptozotocin and fed HFD (hyperlipidemic and hyperglycemic , HGHCi). **A**: Venn diagram showing overlap of genes significantly changed in HGHCi or HCi mice in relation to gene expression in control mice. **B:** Heat map summarizing differentially expressed gene (DEGs) identified by RNA sequencing and DEGs related biological processes using Gene Ontology and EnrichR analysis. Gene count values larger than the average are represented in yellow, while lower counts than the average are represented in blue. Whenever transcript values are close to the control value, samples are colored in white. **C, D**: Heat maps showing list of DEGs related to inflammatory response and collagen degradation pathways, using Gene Ontology and EnrichR analysis. Gene count values larger than the average control are represented in yellow, while lower counts than the average control are represented in blue. Whenever transcript values are close to the control value, samples are colored in white.

Figure 5

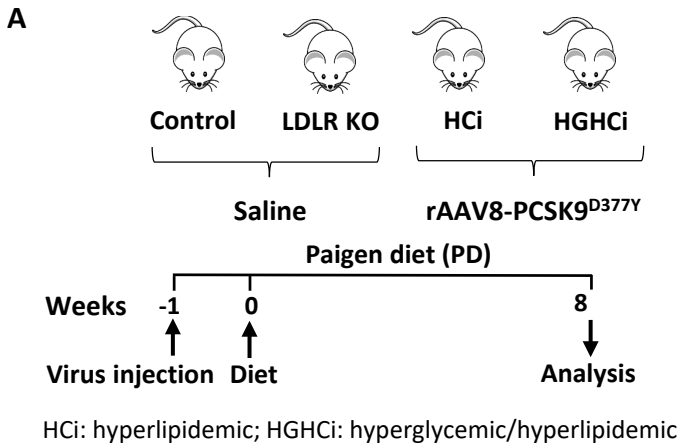

HCi: hyperlipidemic; HGHCi: hyperglycemic/hyperlipidemic

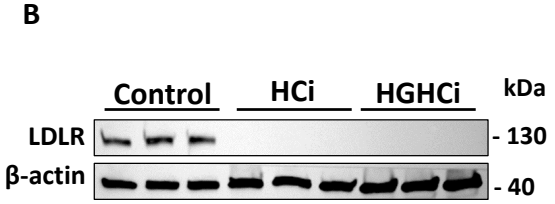

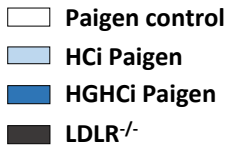

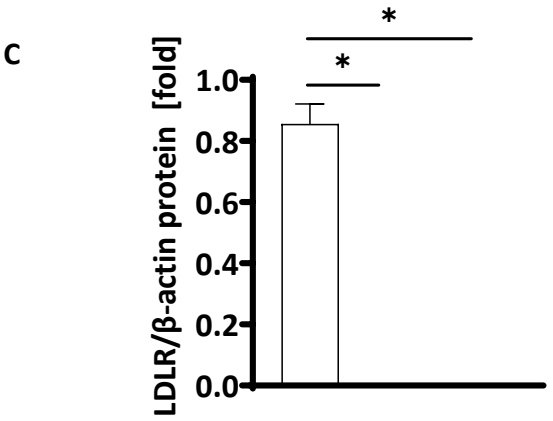

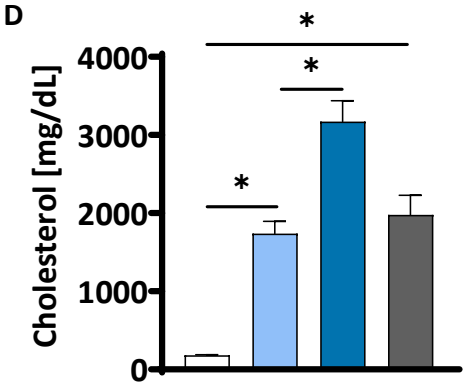

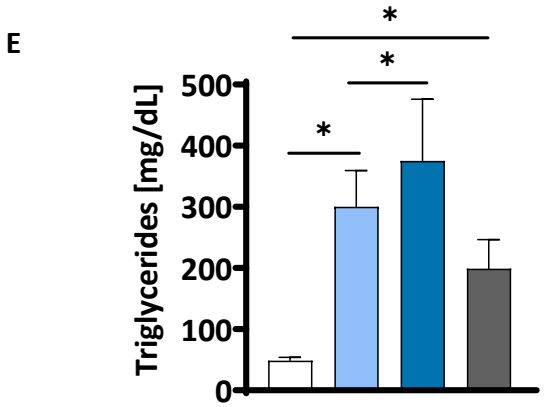

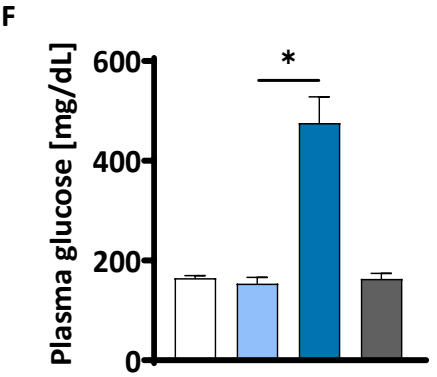

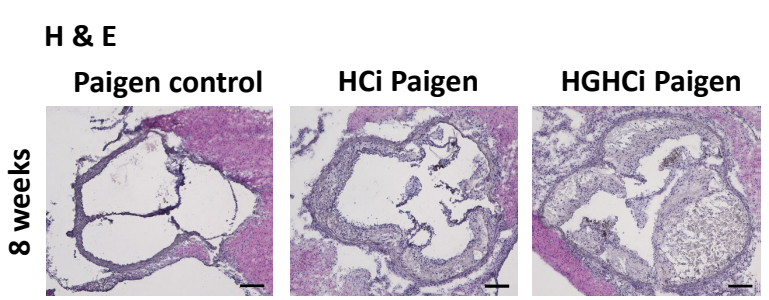

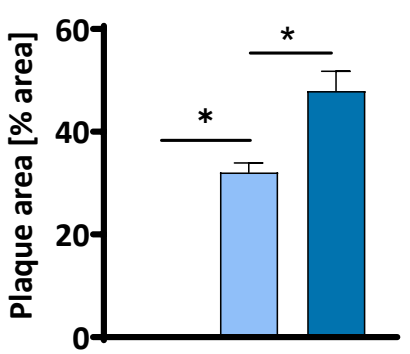

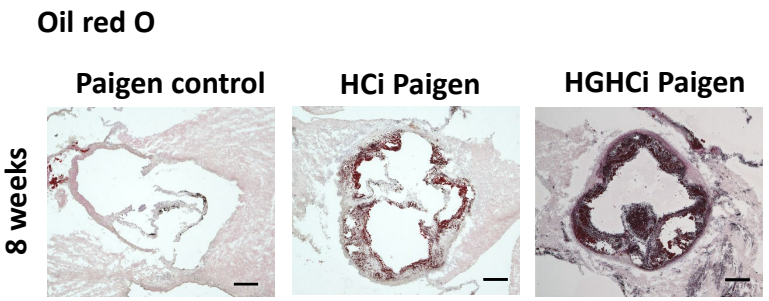

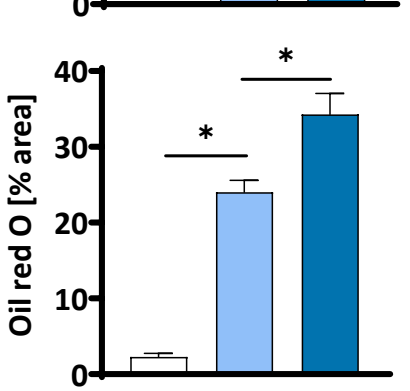

Figure 5: Paigen diet accelerates plaque formation after 8 weeks in the rAAV8-PCSK9 streptozotocin induced hyperglycemic atherosclerosis mouse model. A: Schematic summary of the experimental setup. Mice were analyzed after 8 weeks of interventions initiation. **B**: Representative immunoblot showing hepatic protein levels of low-density lipoprotein receptor (LDLR). β-actin was used as loading control and bar graphs summarizing data. Data were normalized on control mice which were set at 1 (**C**). Bar graphs summarizing data of plasma cholesterol level [mg/dL, **D**], triglycerides [mg/dL, **E**) , and blood glucose levels [mg/dL, **F**]. **G-J:** Representative histological images showing aortic root sections stained with Hematoxylin Eosin (H & E, **G**) and bar graphs summarizing data (**H**). Representative histological images showing aortic root sections stained with Oil-red-O (**I**) and bar graphs summarizing data (**J**). Data presented as mean ± SEM and one-way ANOVA was performed with Sidak's multiple comparison post-hoc test (*$p < 0.05$). Scale bar 200 µm. Paigen control (N=6), HCi Paigen (N=6), HGHCi Paigen (N=6). Control: Wild type mice without rAAV8-PCSK9^{D377Y} injection on paigen diet (PD); HCi Paigen: mice injected with rAAV8-PCSK9^{D377Y} and fed PD (hyperlipidemic); HGHCi Paigen: mice injected with both rAAV8-PCSK9^{D377Y} and streptozotocin and fed PD (hyperlipidemic and hyperglycemic).

Figure 6

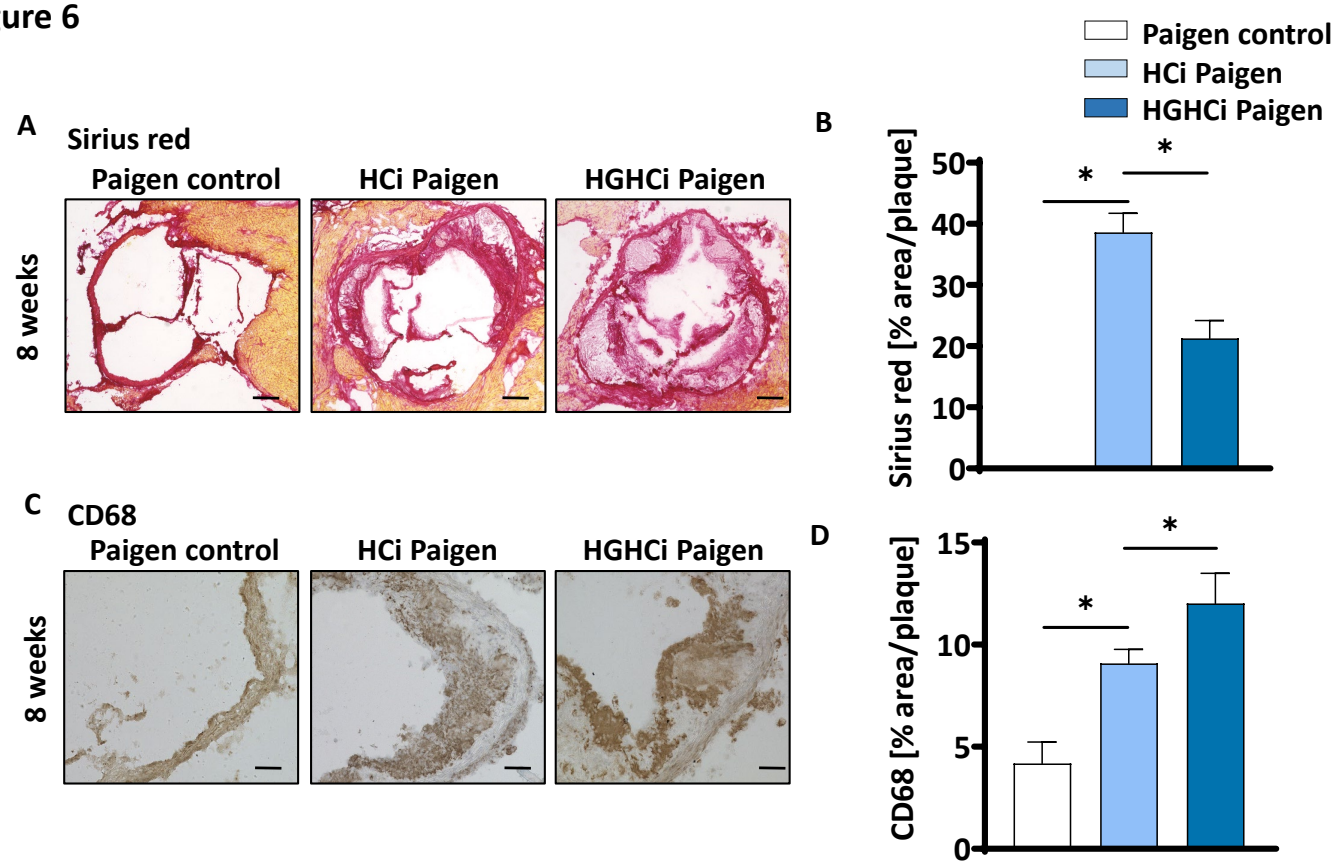

Figure 6: Hyperlipidemic and hyperglycemic mice fed a Paigen diet (PD) show an increased macrophage infiltration within aortic plaques compared to hyperlipidemic mice. **A**: Representative images showing picrosirius red staining for collagen in aortic root sections nd bar graphs summarizing data (**B**). Scale bar 200 µm. **C:** Representative images showing immunohistochemical staining of aortic root sections for macrophages marker CD68 (positive cells detected by HRP-DAB reaction, brown) and bar graphs summarising data (**D**). Data presented as mean ± SEM and one-way ANOVA was performed with Sidak's multiple comparison post-hoc test (*$p < 0.05$). Scale bar 100 µm. Paigen control (N= 7), HCi (N= 4), HGHCi Paigen (N=4). Control Paigen: Wild type mice without rAAV8-PCSK9^{D377Y} injection on paigen diet (PD); HCi Paigen: mice injected with rAAV8-PCSK9^{D377Y} and fed PD (hyperlipidemic, HCi); HGHCi Paigen: mice injected with both rAAV8-PCSK9^{D377Y} and streptozotocin and fed PD (hyperlipidemic and hyperglycemic).

Supplementary Material

Content:

Supplementary Table 1. Characteristics of mice cohort.

Supplementary Figure I. PD fed HGHCi mice showed higher mortality than HFD fed mice.

Supplementary Figure II. Comparison with HFD fed LDLR KO mice.

Supplementary Figure III. Comparison with Paigen fed LDLR KO mice.

Supplementary Figure IV. Hyperglycemia alone does not affect plasma cholesterol levels in mice fed a Paigen diet.

Major resources table

Supplementary Table 1. Characteristics of mice cohort.

High-fat diet	Body weight [g]	Liver weight [g]	Liver/body weight ratio
12 weeks			
Normal chow	31.8 ± 3.7[a]	1.5 ± 0.4[a]	0.04
Saline HFD	40.4 ± 2.3	2.8 ± 0.5	0.06
HCi HFD	39.1 ± 3.3	2.6 ± 0.5	0.07
HGHCi HFD	24.7 ± 0.9[b]	2.8 ± 0.2	0.11
LDLR KO HFD	36.3 ± 5.5	2.1 ± 0.6	0.05
20 weeks			
Normal chow	32.5 ± 2.8[a]	1.7 ± 0.1[a]	0.05
Saline HFD	42.6 ± 4.8	3.0 ± 1.1[b]	0.07
HCi HFD	45.3 ± 3.9[c]	4.1 ± 0.7[ac]	0.09
HGHCi HFD	27.3 ± 3.5[b]	2.7 ± 0.2[b]	0.10
LDLR KO HFD	39.2 ± 3.4	3.2 ± 0.7[c]	0.08

Paigen diet	Body weight [g]	Liver weight [g]	Liver/body weight ratio
8 weeks			
Saline PD	31.1 ± 1.2	2.0 ± 0.1	0.06
HCi Paigen	32.0 ± 3.5	1.7 ± 0.2	0.05
HGHCi Paigen	19.7 ± 3.1[b]	2.7 ± 0.1[b]	0.14
LDLR KO Paigen	27.9 ± 1.6[b]	1.6 ± 0.2	0.06

Supplementary Table 1. Data are shown as mean ± SEM and statistical comparisons between the groups were calculated using the one-way ANOVA and Sidak's posthoc test. [a] $p<0.05$ vs Saline HFD, [b] $p<0.05$ vs HCi HFD, [c] $p<0.05$ vs 12 weeks. HFD: high-fat diet; HCi: hyperlipidemia model; HGHCi: hyperglycemia + hyperlipidemia model; PD: Paigen diet

Supplementary Figure I. PD fed HGHCi mice showed higher mortality than HFD fed mice.

A

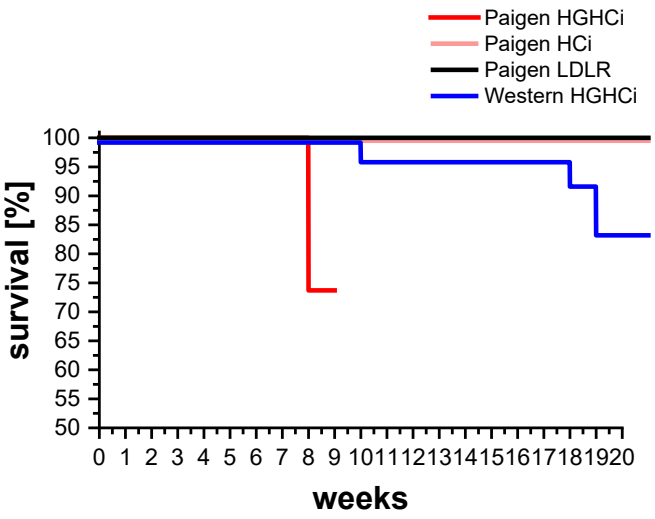

Supplementary Figure I. A: Kaplan-Meier survival curves of HGHCi, HCi and LDL receptor KO mice on Paigen diet compared to HGHCi mice on Western diet (high-fat diet, HFD).

Supplementary Figure II. Comparison with HFD fed LDLR KO mice.

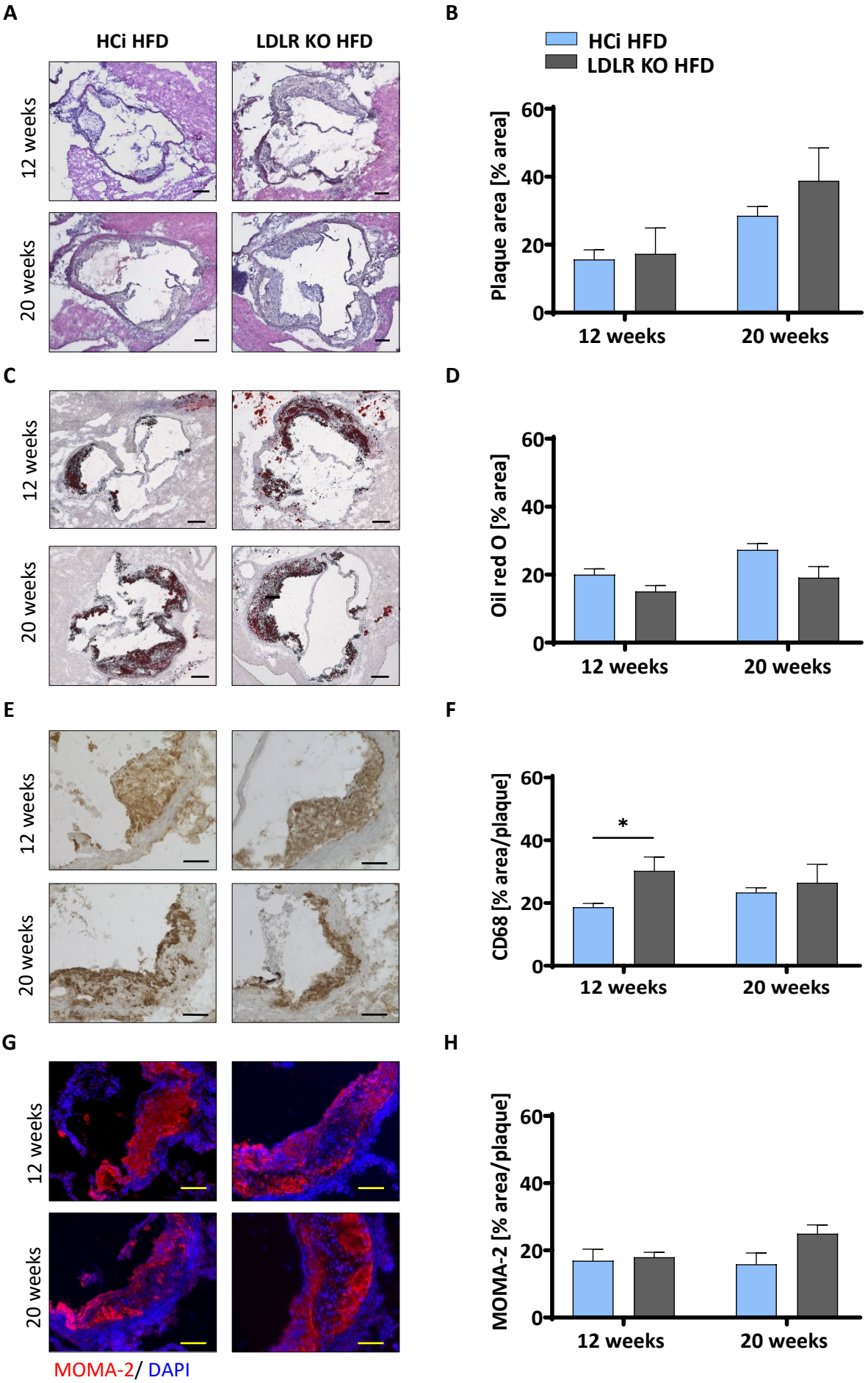

Supplementary Figure II. Comparison with HFD fed LDLR KO mice. A-H: Representative histological images showing aortic root sections stained with Hematoxylin Eosin (H & E, **A**) and bar graphs summarizing data (**B**). Representative histological images showing aortic root sections stained with Oil-red-O (**C**) and bar graphs summarizing data (**D) E:** Representative images showing immunohistochemical staining of aortic root sections for macrophages marker CD68 (positive cells detected by HRP-DAB reaction, brown) and bar graphs summarizing data (**F**). Representative images showing immunofluorescence staining of aortic root sections for macrophages marker MOMA-2 (**G,** MOMA-2, red; DAPI nuclear counterstain, blue) and bar graphs summarizing data. Stainings are imaged at 20 × magnification, Scale bar 100 μm.

Supplementary Figure III. Comparison with Paigen fed LDLR KO mice.

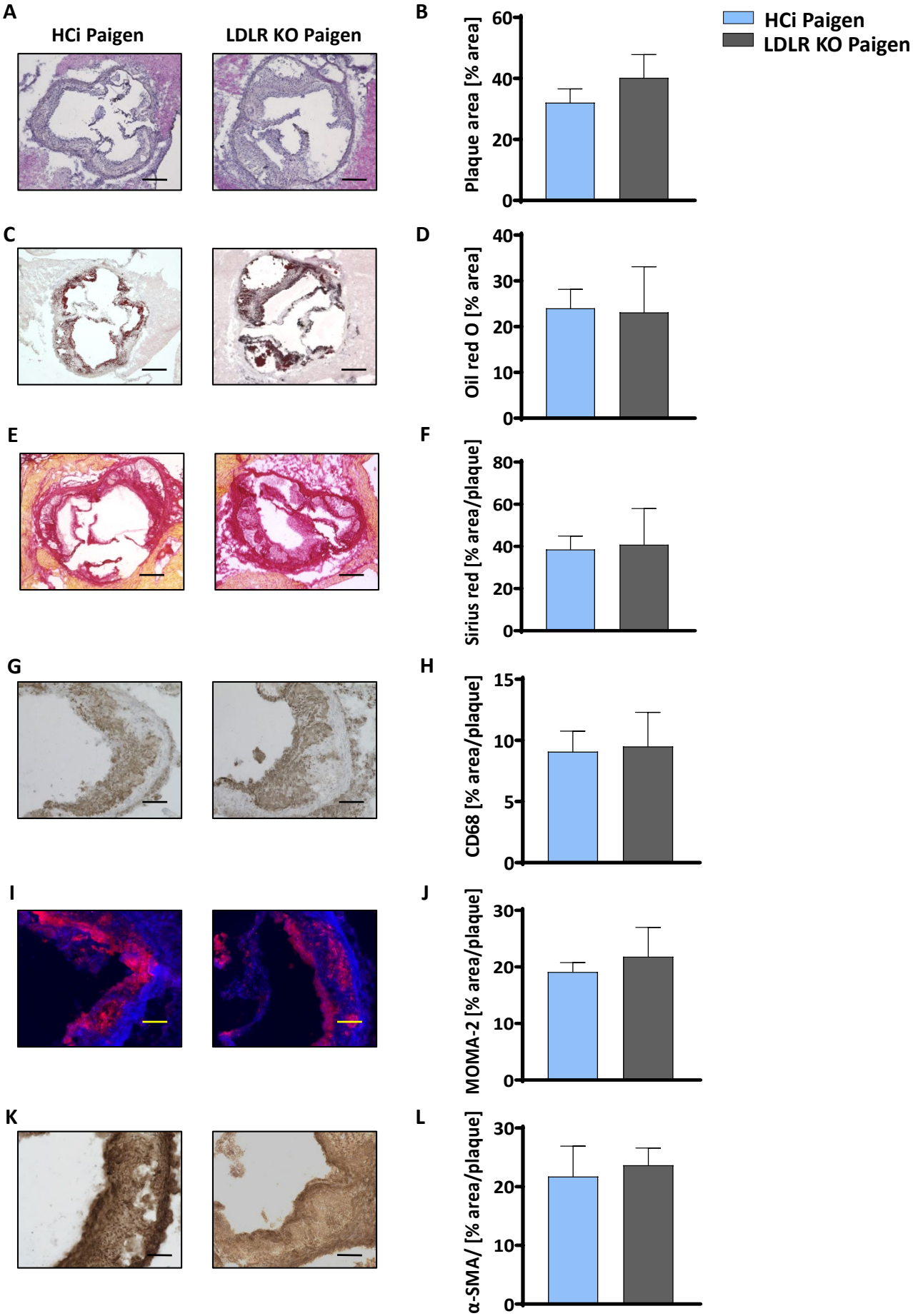

Supplementary Figure III. Comparison with Paigen diet fed LDLR KO mice. A-L: Representative histological images showing aortic root sections stained with Hematoxylin Eosin (H & E, **A**) and bar graphs summarizing data (**B**). Representative histological images showing aortic root sections stained with Oil-red-O (**C**) and bar graphs summarizing data (**D).** Representative histological images showing aortic root sections stained with Sirius Picric Red (**E**) and bar graphs summarizing data (**F) G:** Representative images showing immunohistochemical staining of aortic root sections for macrophages marker CD68 (positive cells detected by HRP-DAB reaction, brown) and bar graphs summarizing data (**H**). Representative images showing immunofluorescence staining of aortic root sections for macrophages marker MOMA-2 (**I,** MOMA-2, red; DAPI nuclear counterstain, blue) and bar graphs summarizing data. Stainings are imaged at 20 × magnification, Scale bar 100 μm (**J**). **K:** Representative images showing immunohistochemical staining of aortic root sections for macrophages marker alpha smooth muscle actin (positive cells detected by HRP-DAB reaction, brown) and bar graphs summarizing data (**L**).

Supplementary Figure IV. Hyperglycemia alone does not affect plasma cholesterol levels in mice fed a Paigen diet.

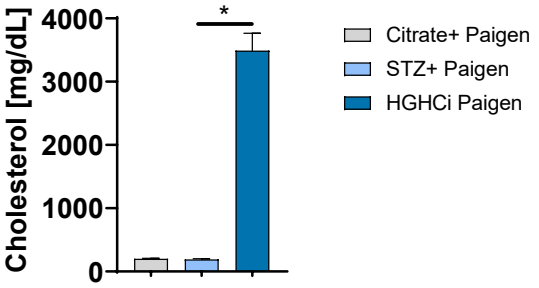

Supplementary Figure IV. Hyperglycemia alone does not affect plasma cholesterol levels in mice fed a Paigen diet. Comparison of cholersterol levels in HGHCi mice (N=13), streptozotocin (STZ) treated mice (N=5) and citrate controls (N=3) fed with Paigen diet. Plasma cholesterol leves [mg/dL] were analyzed 12 weeks after induction of hypergylcemia with STZ.

Major Resources Table

In order to allow validation and replication of experiments, all essential research materials listed in the Methods should be included in the Major Resources Table below. Authors are encouraged to use public repositories for protocols, data, code, and other materials and provide persistent identifiers and/or links to repositories when available. Authors may add or delete rows as needed.

Animals (in vivo studies)

Species	Vendor or Source	Background Strain	Sex	Persistent ID / URL
Mouse	Charles River Laboratories	C57BL/6N	male	C57BL/6 Mouse | Charles River Laboratories. (criver.com)

Genetically Modified Animals

	Species	Vendor or Source	Background Strain	Other Information	Persistent ID / URL
Parent - Male	Mouse	The Jackson Laboratory	000664 C57BL/6J	B6.129S7-Ldlrtm1Her/J Stock No: 002207	https://www.jax.org/strain/002207
Parent - Female	Mouse	The Jackson Laboratory	000664 C57BL/6J	B6.129S7-Ldlrtm1Her/J Stock No: 002207	https://www.jax.org/strain/002207

Antibodies

Target antigen	Vendor or Source	Catalog #	Working concentration	Lot # (preferred but not required)	Persistent ID / URL
mLDLR	R&D System, United States	AF2255	1:200		https://www.rndsystems.com/products/mouse-ldlr-antibody_af2255
mβ-actin	Abcepta Inc., United States	AM1829B	1:10,000		https://www.abcepta.com/products/AM1829b-Beta-Actin-Antibody
Goat IgG HRP	Agilent Technologies, United States	P0449	1:1,000		https://www.agilent.com/store/en_US/LCat-SubCat3ECS_244797/Rabbit-Anti-Goat-Immunoglobulins-HRP
Mouse IgG HRP	Agilent Technologies, United States	P0447	1:10,000		https://www.agilent.com/en/product/immunohistochemistry/antibodies-controls/secondary-antibodies/goat-anti-mouse-immunoglobulins-hrp-(affinity-isolated)-153239
mMOMA-2	abcam, Germany	ab33451	1:100		https://www.abcam.com/monocyte--macrophage-antibody-moma-2-ab33451.html

DOI [to be added]

mCD68	abcam, Germany	ab125212	1:1,000		https://www.abcam.com/cd68-antibody-ab125212.html
Mouse alpha smooth muscle actin (mα-SMA)	abcam, Germany	ab124964	1:250		https://www.abcam.com/alpha-smooth-muscle-actin-antibody-epr5368-ab124964.html
Rat IgG Alexa Fluor 568	ThermoFisher, United States	A-11077	1:100		https://www.thermofisher.com/antibody/product/Goat-anti-Rat-IgG-H-L-Cross-Adsorbed-Secondary-Antibody-Polyclonal/
anti-rabbit HRP	Vector Laboratories, Inc., Unites States	MP-7801			https://vectorlabs.com/immpress-horse-anti-rabbit-igg-plus-polymer-kit-peroxidase.html

DNA/cDNA Clones

Clone Name	Sequence	Source / Repository	Persistent ID / URL

Cultured Cells

Name	Vendor or Source	Sex (F, M, or unknown)	Persistent ID / URL

Data & Code Availability

Description	Source / Repository	Persistent ID / URL

Other

Description	Source / Repository	Persistent ID / URL
BCA reagent	Perbio Science, Germany	
Vectashield mounting medium with DAPI	Vector Laboratories, United States	
Nitrocellulose membrane	Bio-Rad, USA	
Immobilon™ western chemiluminescent HRP substrate	Merck, Millipore, United States	
Streptozotocin	Enzo Life Sciences, Germany	
Oil-Red O	Sigma-Aldrich, Germany	
Accu-chek test strips	Roche Diagnostics, Germany	
Accu-check glucometer	Roche Diagnostics, Germany	
Protease inhibitor cocktail	Roche Diagnostics, Germany	
Albumin fraction V	Carl ROTH, Germany	
Hematoxylin Gill II	Carl ROTH, Germany	

DOI [to be added]

Acrylamide	Carl ROTH, Germany	
Agarose	Carl ROTH, Germany	
Aqueous mounting medium	ZYTOMED, Germany	
High fat diet	Ssniff, Germany	
PBS	Life Technologies, Germany	
Rompun	Bayer, Germany	
Ketamine	Beta-pharm, Germany	

DOI [to be added]